Elevated local senescence in diabetic wound healing is linked to pathological repair via CXCR2

Journal:	*Journal of Investigative Dermatology*
Manuscript ID	JID-2018-0663.R2
Article Type:	Original Article
Date Submitted by the Author:	n/a
Complete List of Authors:	Wilkinson, Holly; Hull York Medical School, Centre for Atherothrombosis and Metabolic Disease Clowes, Christopher; University Hospitals of North Midlands NHS Trust, Research and Development Department Banyard, Kayleigh; Hull York Medical School, Centre for Atherothrombosis and Metabolic Disease Matteucci, Paolo; Hull and East Yorkshire Hospitals NHS Trust, Plastics Department Mace, Kimberly; University of Manchester, Division of Cell Matrix Biology & Regenerative Medicine; University of Manchester Hardman, Matthew; Hull York Medical School, Centre for Atherothrombosis and Metabolic Disease
Keywords:	Aging, Keratinocytes, Macrophages, Wound Healing

Title: Elevated local senescence in diabetic wound healing is linked to pathological repair via CXCR2.

Running Title: Senescence in diabetic wound healing.

Authors: Holly N. Wilkinson[1], Christopher Clowes[2], Kayleigh L. Banyard[1], Paolo Matteuci[3], Kimberly Mace[4] and Matthew J. Hardman[1*]

[1]Centre for Atherothrombosis and Metabolic Disease, Hull York Medical School, The University of Hull, HU6 7RX, United Kingdom.

[2] Research and Development Department, Royal Stoke University Hospital, University Hospitals of North Midlands NHS Trust, ST4 6QG, United Kingdom.

[3]Hull and East Yorkshire Hospitals NHS Trust, United Kingdom.

[4] Faculty of Biology, Medicine and Health, The University of Manchester, M13 9PT, United Kingdom.

ORCID IDs

Holly N. Wilkinson - https://orcid.org/0000-0002-8453-7264

Christopher Clowes - https://orcid.org/0000-0001-7525-5161

Kayleigh L. Banyard - https://orcid.org/0000-0003-1175-6017

Paolo Matteucci - https://orcid.org/0000-0002-0594-1577

Kimberly Mace - https://orcid.org/0000-0002-3184-878X

Matthew J. Hardman - https://orcid.org/0000-0002-6423-5074

***Corresponding author:**

Matthew J. Hardman

Address: University of Hull, Daisy Building (2nd Floor), Castle Hill Hospital, Hull, HU16 5JQ.

Phone Number: 01482 461879

Email: m.hardman@hull.ac.uk

1

Abbreviations: Db (diabetic), SASP (senescence associated secretory phenotype), Mφ (macrophage).

ABSTRACT

Cellular senescence can be broadly defined as a stable, yet essentially irreversible, loss of proliferative capacity. Historically, senescence is described as a negative outcome of advanced cellular age. It is now clear, however, that senescence represents a dynamic autonomous stress response, integral to long-term tumour suppression. Intriguingly, transient induction of a senescent phenotype has actually been suggested to promote regeneration in both liver and skin. Here we explored the role of senescence in pathological aged and diabetic murine wound healing. Aged and diabetic wounds possessed greater numbers of senescent cells, while diabetic macrophages maintained altered retention of polarisation and produced a CXCR2-enriched SASP. Of translational relevance, targeted expression of CXCR2 in primary human dermal fibroblasts led to paracrine induction of nuclear p21. Further, a selective agonist to CXCR2 was able to reverse delayed healing in diabetic mice and accelerate *ex vivo* human skin wound healing. Collectively these data suggest a hitherto unappreciated role for CXCR2 in mediating cellular senescence in pathological wound repair.

Key Words: Senescence, Wound Healing, Ageing, Diabetes, Macrophage Polarisation.

INTRODUCTION

Cellular senescence, first described by Hayflick and Moorhead (1961), is broadly defined as a stable yet essentially irreversible loss of cellular proliferative capacity (Demaria et al, 2014; Jun and Lau, 2010). A wealth of evidence supports senescence as an autonomous anti-cancer mechanism, evolved to halt incipient neoplastic cellular transformation in young organisms (Campisi and Robert, 2014). Intriguingly, senescent cells are also apparent in noncancerous situations (e.g. fibrosis) and accumulate during ageing (Campisi and di Fagagna, 2007; Jun and Lau, 2010), yet the direct role of senescence in ageing and subsequent disease states remains to be fully elucidated.

Senescent cells show flattened morphology and accumulate with chronological age (Campisi and di Fagagna, 2007). Senescence is induced by a number of age-related mechanisms, including repeated cell division (reviewed in Tchkonia et al, 2013), telomere shortening and increased reactive oxygen species (ROS; Di Micco et al, 2006; Passos et al, 2010). Successive activation of anti-tumorigenic networks is controlled at the nexus by the p53 transcriptional regulator. p53 directly transactivates the proliferation inhibitor, p21 (He et al, 2007), therefore preventing cyclin dependent kinase (CDK) 2-mediated pRb (retinoblastoma protein) inactivation (Beauséjour et al, 2003). Similarly, p16 transcription prevents CDK4 and CDK6-mediated phosphorylation of pRb (Takahashi et al, 2006). As pRb naturally binds to E2F/DP transcription factor complexes (Dimova and Dyson, 2005), failure to phosphorylate pRB inhibits transcription of E2F target genes (Narita et al, 2003; Malumbres and Barbacid, 2005); hence, progression from the G1 to S phases is prevented. Despite species-specific differences, both p21 and p16 have strong causal links with human ageing (Berry et al, 2017; Peng et al, 2015; Kim et al, 2015) and murine experimental models (Baker et al, 2008; Baker et al, 2011; Choudhury et al, 2007).

Although unable to divide, senescent cells remain metabolically active. They do so via a SASP (senescence-associated secretory phenotype), demonstrated by an increase in the secretion of pro-inflammatory cytokines (e.g. the interleukins IL-1a, IL-6, IL-8), growth factors (transforming growth factor, TGF-β) and proteases (matrix metalloproteinases, MMPs) that actively alter the tissue microenvironment (Freund et al, 2010). The SASP feature of senescent cells is a DNA damage response (DDR), and as a result, heavily contributes to age-related functional decline (Rodier et al, 2009). More recently, senescence has been experimentally manipulated to discover its causal roles in driving progeroid pathology (Baker et al, 2011; Baker et al, 2016).

The SASP is also implicated in the aetiology of many chronic diseases (e.g. atherosclerosis, Erusalimsky and Kurz, 2005), by allowing low abundance senescent cells to exert strong, local tissue effects. For example, the presence of an obesity-driven pro-inflammatory SASP (Schafer et al, 2016) has been suggested to mediate insulin resistance and the development of type II diabetes mellitus (T2DM) in both mice (Minamino et al, 2009) and humans (Spranger et al, 2003). Interestingly, fundamental roles for macrophages (Mφs) in mediating this "metainflammation", or metabolically driven inflammation, have been elucidated. Here, many Mφ-specific cytokines form part of the SASP (e.g. MCP-1; Kamei et al, 2006; Prattichizzo et al, 2018; Xu et al, 2003), while SASP components are known to act on classical Mφ receptors (e.g. CXCR1, CXCR2, CX3CR1, reviewed in Sagiv and Krizhanovsky, 2013).

As described, senescence is a stochastic chronic mechanism related to ageing and pathology, but a handful of studies have demonstrated the importance of damage-induced senescence in arbitrating wound healing (e.g. Demaria et al, 2014; Jun and Lau, 2010). Wound-induced senescence remains transient, as following tissue repair, senescent cells are cleared via immunosurveillance (Childs et al, 2014). Mφs also play a crucial role in facilitating tissue repair by mediating granulation, angiogenesis and remodelling events (reviewed in Koh and DiPietro,

2011). Mφs switch from a pro-inflammatory (M1-like) state to a pro-healing (M2-like) state to aid wound resolution. However, in models of delayed healing, such as diabetes, a heightened pro-inflammatory Mφ response is observed (Bannon et al, 2013; Khanna et al, 2010). Due to their association with the SASP, it is likely that Mφs may retain key involvement in the senescence aspect of cutaneous wound healing.

Given the previously described link between the pro-inflammatory SASP and diabetes, we sought to characterise hallmark senescence biomarkers in diabetic murine skin and wounds. As Mφs are implicated as one of the main sources of the SASP in diabetes, we next screened diabetic Mφs for specific SASP components and evaluated their function. Finally, we revealed the translational relevance of blocking an explicated diabetic SASP receptor to promote wound closure.

RESULTS

Senescent cells accumulate in pathological skin and wounds. To evaluate the senescent phenotype in skin (D0) and wounds (D7) from normal (young) and delayed healing (Db and aged) mice, we first performed SA-βGAL staining (**Figure 1A-B**). Here, the number of SA-βGAL+ve cells was greatest in aged dermis ($P < 0.001$). Interestingly, modest increases in dermal ($P = 0.06$) SA-βGAL were also visualised in the Db model. We next asked whether acute injury induces abnormal accumulation of senescent cells in pathological wounds. Here, levels of SA-βGAL+ve cells increased more than 2-fold in Db ($P < 0.05$) and aged ($P < 0.01$) wounds at day 7 post-injury, compared to young controls. Increased p16-specific senescence was also confirmed in Db wounds (**Supplementary Figure S1**). Further, qRT-PCR revealed substantially greater levels of the senescence genes, *Cdkn1b* (p27; $P < 0.05$), *Cdkn2a* (p16; $P < 0.01$) and *Trp53* (p53; $P < 0.01$) in aged skin (**Figure 1D, E, F**, respectively**).** Interestingly, *Cdkn1a* was upregulated following injury in Db versus young wounds (p21; $P < 0.05$; **Figure 1C**), and *Cdkn1b* ($P < 0.05$), *Cdkn2a* ($P < 0.05$) and *Trp53* ($P < 0.01$) showed a trend towards

increase in Db wounds. By contrast, no significant changes in senescent genes were apparent between young and aged wounds (**Figure 1**). These data demonstrate for the first time that senescent cells rapidly accumulate following injury in Db mouse skin, and suggest a potential crossover between diabetes and aging wound pathology.

The heightened macrophage response in diabetic wounds is intrinsically skewed to senescence and M1 polarisation. Db murine wounds are extensively used as an archetypical delayed healing model (reviewed in Ansell et al, 2012). Histological assessment via Masson's trichrome staining confirmed delayed healing (larger wounds) in Db (**Figure 2A-B**) versus NDb controls at day 7 post-injury. Intriguingly, a large proportion of the senescent cells in Db wounds were Mφs, which were highly senescent compared to NDb Mφs ($P < 0.001$; **Figure 2C-D**). Mφs are implicated in playing a major role in senescence and metainflammation (reviewed in Sagiv and Krizhanovsky, 2013). Thus, bone-marrow derived Mφs were isolated from NDb and Db mice, polarised with M1 and M2 cytokines, and characterised for a potential senescent phenotype via SA-βGAL staining. Here, a higher number of Db Mφs were SA-βGAL positive than NDb Mφs (**Figure 2E-F**, $P < 0.001$), while qRT-PCR demonstrated significantly increased *Cdkn1a* and *Cdkn2a* in Db M1-polarised Mφs ($P < 0.05$ and $P < 0.01$, respectively), and increased *Cdkn1a* in Db M2-polarised Mφs ($P < 0.001$; **Figure 2G**). As expected, M1-stimulated Mφs displayed elevated *Nos2*, while *Ym1* levels were upregulated in M2-stimulated Mφs (**Figure 2G**). However, the overall expression of both *Nos2* ($P < 0.001$) and *Ym1* ($P < 0.01$) was significantly reduced in Db Mφs at 72 hours post-stimulation (**Figure 2G**), At the protein level, Db Mφs also displayed reduced polarisation (less Nos2 and Arg1 staining) and increased expression of the senescence marker p21 (**Figure 2H**).

Diabetic macrophage SASP is enriched in CXCR2 ligands that selectively induce chemokine and fibrotic markers in fibroblasts. Given that delayed wound healing is characterised by deleterious alterations in Mφ function (Bannon et al, 2013), while heightened

senescence is observed in Db M1 and M2 polarised Mφs, we next profiled the Db Mφ SASP using antibody arrays designed to detect a number of SASP-relevant soluble factors (**Figure 3A-B**). For visualisation, the data were displayed as Db versus NDb fold changes. A number of secreted factors were upregulated in Db M2-stimulated Mφs, including the previously reported SASP components CXCL1, RANTES, CXCL2, MIP-1α, TNF-α, IL-1ra and TIMP-1 (Chien et al., 2011). qRT-PCR also confirmed upregulation of the key SASP components *Cxcl1* ($P < 0.05$) and *Cxcl2* at the mRNA level, and upregulation of their common receptor, *Cxcr2* ($P < 0.05$) in Db Mφs (**Figure 3C**). Further, gelatin zymography revealed increased activity of the gelatinase, MMP-2, in Db M0 and M2-stimulated CM ($P < 0.05$, **Figure 3D**; un-enhanced gel **Supplementary Figure S2**). Moreover, returning to normal and pathological wound tissue, *Cxcl1* ($P < 0.001$; **Figure 3E**), *Cxcl2* ($P < 0.05$; **Figure 3F**) and their common receptor, *Cxcr2* ($P < 0.05$; **Figure 3G**), were all significantly elevated in Db wounds, but not in aged wounds (versus young).

Previously, a mesenchymal SASP has been shown to influence fibroblast differentiation during wound repair (Demaria et al, 2014). Given the similarities between mouse and human fibroblast SASP components (Coppé et al, 2010), we next determined the effect of CM from NDb and Db murine Mφs on HDF gene expression profile (**Figure 3H**). Looking at early gene expression changes, Db CM did not significantly alter p16 (*CDKN2A*), p21 (*CDKN1A*) or *NFE2L2* (NRF2; oxidative stress marker; Nguyen et al., 2009) expression in young or aged HDFs, indicating no direct induction of fibroblast senescence markers. However, Db CM increased *SERPINE1* (PAI-1), a well-known marker of fibrosis and fibroblast senescence (Kortlever et al, 2006), in both aged and young HDFs, and *COL1A1* (collagen type I alpha chain I) in aged HDFs. Curiously, *COL3A1* (collagen type III alpha chain I; an early injury matrix protein) was downregulated in young and aged HDFs by Db CM. Together these data suggest that Db CM favours a pro-fibrotic fibroblast phenotype. Finally, Db CM from M1-polarised Mφs strongly

induced *CXCL1* and *CXCL2* in young and aged HDFs, while M2-polarised Db CM significantly induced *CXCL2* in aged HDFs alone ($P < 0.01$).

Ectopic expression of CXCL2 potentiates CXCL2 induction and p21 nuclear localisation in non-transfected fibroblasts. As CXCL1/2-rich CM from Db Mφs promotes paracrine induction of CXCR2 ligands in HDFs, we next looked at the effect of direct transfection of CXCL2 in HDFs. As expected, fibroblasts transfected with a CXCL2 plasmid exhibited significantly higher CXCL2 expression at 2 days ($P < 0.05$) and 6 days ($P < 0.001$) post-transfection (than controls, **Figure 4A-B**), suggesting clear paracrine induction of CXCL2. Intriguingly, by D6, CXCL2-transfected fibroblasts also exhibited higher levels of nuclear p21 ($P < 0.001$; **Figure 4C-D**), which is associated with senescence (e.g. in endothelial cells, Matthaei et al., 2012), and higher SA-βGAL and p16 expression (supplementary **Figure S3**). As YFP+ve fibroblasts did not increase between D2 and D6 post-transfection (**Figure 4E**), these data suggest that CXCL2 exerts strong local paracrine effects that promote senescence induction. Further, transfected HDFs produced a SASP-rich secretome (**Figure 4F-G**) which displayed heightened MMP2 activity (**Figure 4H-I**, un-cropped gel **Supplementary Figure S4**), while intracellular expression of *MMP2* and *COL3A1* was increased following CXCL2 transfection (**Figure 4J**).

Human wound healing is accelerated by blockade of the CXCR2 receptor. CXCL2 secretion is increased in Db Mφs (**Figure 3**), CXCL2 induces senescence in HDFs (**Figure 4**), and increased senescence is linked to diabetic wound healing. We thus tested the effect of CXCL2 receptor (CXCR2; Acosta et al, 2008) activation/inhibition during human healing. Treatment of human keratinocyte (HaCaT) scratch wounds with the ligands, CXCL1 and CXCL2, led to a delay in closure ($P < 0.05$ and $P < 0.01$ respectively), while blockade of CXCR2 (SB265610; Bradley et al, 2009) significantly improved ($P < 0.05$) scratch wound repair (**Supplementary Figure S5**). To confirm specificity co-treatment with SB265610 and

either CXCL1 or CXCL2 was performed, with the effect of both chemokines completely blocked. Interestingly, when the two ligands (CXCL1 and CXCL2) were combined they were able to delay wound closure, even in the presence of SB265610 ($P < 0.001$).

Human *ex vivo* wounds were subjected to the same treatments. Here, combinatorial treatment with CXCL1 and CXCL2 delayed wound closure ($P < 0.05$; **Figure 6A, C**; K14 staining), while application of SB265610 increased healing ($P < 0.01$). In the presence of SB265610, CXCL1 treatment ($P < 0.05$), and treatment with both ligands ($P < 0.05$), delayed epidermal wound healing. Intriguingly, combining SB265610 and CXCL2 rescued delayed wound closure observed with CXCL2 treatment alone, thus suggesting SB265610 to be selective for CXCL2 *ex vivo*. Finally, neo-epidermal proliferation (K6 staining**, Figure 6B, D**) was significantly impaired only in wounds co-treated with SB265610 and CXCL1 ($P < 0.05$), further demonstrating SB265610 to be less effective against CXCL1 than CXCL2 (full set of representative images is provided in **Figure S6**). Together, these data clearly show that blocking the canonical senescence receptor, CXCR2, promotes human epidermal wound closure.

CXCR2 antagonist treatment reduces wound size, inflammation and macrophage senescence during diabetic wound healing. We next returned to the diabetic mouse model, where we assessed the effect of blocking CXCR2 receptor on delayed-healing diabetic wound repair *in vivo*. Diabetic murine wounds were treated with SB265610 or vehicle, and collected at day 7 post-injury. CXCR2 antagonist-treated wounds were significantly smaller than control wounds (width, $P < 0.01$; area, $P < 0.05$; **Figure 6A-C**), with reduced local inflammation (neutrophil numbers; $P < 0.05$; **Figure 6D, G**). Finally, faster healing in SB265610-treated diabetic mouse wounds was associated with a substantial local reduction in senescent macrophages ($P < 0.01$; **Figure 6F, H**). Taken together these data suggest that blocking CXCR2 promotes healing in diabetic wounds by inhibiting local macrophage senescence, reducing local inflammation and promoting wound re-epithelialisation.

DISCUSSION

Although the mechanisms are not fully understood, senescence contributes to age-related dysfunction, partly through regulation of the SASP (Coppé et al, 2008). Additional roles for SASP are emerging in embryogenesis (Storer et al, 2013) and liver regeneration (Jun and Lau, 2010; Krizhanovsky et al, 2008; Yosef et al, 2017), while in normal wound repair, Demaria et al. (2014) identified PDGFA as a wound-derived SASP component driving fibroblast differentiation. In the present study, we focused on the role of senescence in pathological wound repair. For the first time, we demonstrate elevated local senescence in diabetic wound healing.

Senescence and diabetes have previously been linked in other tissues, including pancreatic (Sone and Kagawa, 2005), and adipose (Minamino et al, 2009). Interestingly, young diabetic mice share common features with aged mice, including accumulation of advanced glycation end products (AGEs; Goova et al, 2001) and heightened ER stress (reviewed in Naidoo and Brown, 2012), which promote the onset of premature cellular senescence (Liu et al, 2014). Increased senescence also occurs in the kidney following streptozocin-induced diabetes (Satriano et al, 2010), while removal of p16+ve cells improves islet regeneration and survival following β cell ablation (Krishnamurthy et al, 2006).

To delve deeper into the link between senescence and pathological repair, we focussed on diabetic Mφs which show delayed initial wound infiltration (Bannon et al, 2013), prolonged inflammation (Wood et al, 2014), and reduced M2-polarisation (Mirza et al, 2015). Our data revealed that Db Mφs exhibit: a) reduced polarisation-potential at 72 hours post-cytokine stimulation (lower *Nos2* in M1- and *Ym1* in M2-polarised) and; b) increased expression of *Cdkn1a* and *Cdkn2a*, with expression of known SASP factors (Coppé et al, 2010; Coppé et al, 2008). It has been noted previously that a hyperglycaemic environment promotes senescence induction and SASP production in human Mφs (Prattichizzo et al, 2018), while glucose restriction extends human fibroblast lifespan *in vitro* (Li and Tollefsbol, 2011). Indeed, the anti-

diabetic drug, metformin, reduces SASP in oncogene-induced senescence (Moiseeva et al, 2013). CXCL1 and CXCL2 were identified as the most highly expressed SASP factors in polarised Db Mφs, in line with increased expression of *Cxcr2* and its ligands in Db wound tissue. CXCL2 expression has been previously observed in Db wounds (Wetzler et al, 2000). Previous authors have demonstrated a peak in wound cellular senescence at 6-7 days post-injury in control mice (Demaria et al., 2014), we therefore focussed on this time-point within our study. A limitation of this approach is that it is unable to address temporal changes in wound senescence. However, our combined *in vivo* and *in vitro* findings collectively suggest that CXCR2 ligand upregulation is important for Db wound pathology.

Wound healing involves extensive immune cell, fibroblast cross-talk. For example, NK cells promote pro-inflammatory cytokine and chemokine production in HDFs (Müller et al, 2000). In this study we show that the Db SASP drives a profibrotic phenotype, upregulating *SERPINE1* and *COL1A1* in HDFs. In their landmark paper, Acosta et al (2008) determined CXCR2 and its ligands to be potent mediators of senescence in MEFs and immortalised cells, but they did not consider the potential paracrine effects of the SASP. Here we find that CXCL2 expression in HDFs potentiated over time correlating with nuclear localisation of p21. This supports a paracrine effect for CXCL2, or CXCL2-mediated SASP component(s) in senescence induction. Indeed, we find that both ectopic expression of, and exposure to CXCL2 as part of the SASP, mediate a senescence response in primary human dermal fibroblasts.

Fibroblast senescence is likely a contributing factor to poor healing outcome (Harding et al, 2005) as chronic wound fibroblasts display high senescence (Ågren et al, 1999; Mendez et al, 1998; Stephens et al, 2003; Vande Berg et al, 1998) and a correlation exists between fibroblast senescence and time to heal in chronic wounds (Stanley and Osler, 2001). Here we report that directly inhibiting the senescence mediator CXCR2 (antagonist SB265610; Bradley et al, 2009), significantly increased the rate of wound closure in *in vitro* and *ex vivo* human wound models.

Conversely, ligand treatment (CXCL1 and CXCL2) delayed HaCaT scratch wound closure. Intriguingly, CXCR2 inhibition rescued the effects of CXCL2 *in vitro* and *ex vivo*, yet failed to negate the inhibitory effects of CXCL1, or combinatorial ligand treatment. This likely reflects the fact that CXCL1, but not CXCL2, displays promiscuous receptor activation activity (reviewed in Balkwill, 2012). Curiously CXCR2 activation promotes keratinocyte migration and proliferation (Kroeze et al, 2012), while mice ubiquitously lacking CXCR2 display delayed re-epithelialisation, less wound granulation, impaired neovascularisation (Devalaraja et al, 2000), and diminished immune cell recruitment to wounds (Milatovic et al, 2003). The present data further demonstrated the significance of CXCR2 antagonism in diabetic murine wound healing *in vivo*. Here, SB265610 treatment dampened neutrophil infiltration and reduced macrophage senescence. Thus, it appears that CXCR2 signalling must be tightly regulated for optimum wound repair.

Overall, these data reveal excessive CXCR2 and increased local cellular senescence in delayed healing diabetic wounds, while treatment with a selective CXCR2 antagonist promotes skin repair in human *ex vivo* and diabetic *in vivo* murine wound models. These observations provide the first step towards the future development of chronic wound therapies targeting the CXCR2 receptor and, consequently, wound-induced senescence.

MATERIALS AND METHODS

Animal Experimentation. Wild-type (WT; C57Bl/6), non-diabetic (NDb; Lepr$^{-/+}$) and diabetic (Db; Lepr$^{-/-}$) mice were obtained from Envigo Ltd (UK) and housed in the Biological Services Facility (BSF, The University of Manchester, UK) with *ad libitum* access to food and water. NDb, Db and "young" WT mice were wounded at 8-10 weeks old, while "aged" WT mice were wounded at 80-90 weeks of age. Cages were kept under constant temperature, humidity and a 12-hour light-dark cycle. All animal procedures were carried out according to Home Office regulations.

Wounding Experiments. Mice were anaesthetised and wounded using our established protocol (Ashcroft et al, 2003). Briefly, two equidistant full-thickness 1cm incisional wounds were made on the dorsum of young and aged mice, while two full thickness 6 mm dorsal excisional wounds were created on NDb and Db mice. Mice were administered buprenorphine post-operatively and monitored regularly prior to wound collection at 7 days post-injury (see Supplementary Materials and Methods). For drug treatments, the CXCR2 antagonist, SB265610 (R&D systems, Abingdon, UK), was administered subcutaneously to wounds at 1 mg/kg of animal body weight. Control mice were treated with a vehicle only (1% DMSO in Dulbecco's phosphate buffered saline). Treatments were given at time of wounding, and at day 2 (D2), D4 and D6 post-injury.

Histological Analysis. SA-βGAL (senescence associated β-D-galactosidase) staining and p16 immunohistochemistry was performed to measure senescent cell accumulation in normal skin (D0) and wound tissue (D7). Wound healing analysis was determined with Masson's Trichrome staining and senescent Mφs were stained via immunofluorescence (Supplementary Materials and Methods).

Quantitative real-time PCR (qRT-PCR). RNA was extracted from wounds, normal skin tissue and cells. Primer sequences are provided in the Supplementary Materials and Methods.

Macrophage Activation. Mononuclear phagocyte progenitor cells were isolated from murine bone marrow as described (Supplementary Materials and Methods). On day 7 post-isolation, Mφs were stimulated with LPS (100 ng/ml; Sigma-Aldrich, Suffolk, UK) and IFN-γ (100 ng/ml; Sigma-Aldrich) to become M1-like, with IL-4 (20 ng/ml; Sigma-Aldrich) and anti-IFN-γ (50 μg/ml; 2BScientific, Upper Heyford, UK) to become M2-like and with DMEM and no supplements to remain non-stimulated (M0). Mφs were incubated overnight at 37 ºC with 5 % CO_2 and collected for RNA isolation, immunocytochemistry (Supplementary Materials and Methods), or used for subsequent fibroblast SASP conditioning experiments.

SASP Conditioning. Activation media was aspirated, replaced with fresh Mφ media (w/o L929 CM), and Mφs were incubated at 37 ºC and 5 % CO_2 for 48 hours. Mφ CM and RNA was collected and stored at -80 ºC until use. Primary human dermal fibroblasts (HDFs) were isolated from skin (see Supplementary Materials and Methods) obtained under LREC approval (17/SC/0220) and full informed patient consent. HDFs were isolated from 3 young (< 50 years of age) and 3 aged (> 75 years of age) donors (Supplementary Materials and Methods), treated with Mφ CM for 24 hours at 37 ºC and 5 % CO_2, and collected for RNA.

SASP Characterisation. CM from NDb and Db M1-stimulated and M2-stimulated Mφs was characterised using the Proteome Profiler Mouse Cytokine Array Kit (R&D systems) following manufacturer's instructions. Developed films were imaged and integrated density analysis performed in ImageJ v.1.8 (NIH, US). As the proteome array could not identify the expression of matrix metalloproteinases (MMPs), gelatin zymography was utilised for this purpose (as in Wilkinson et al, 2018).

Transfection. HDFs were transfected with a control plasmid (pUNO1-mcs), or CXCL2-containing plasmid (pUNO1-CXCL2; both InvivoGen, Toulouse, France) using Lipofectamine™ 3000 reagent (Thermo Fisher Scientific) according to manufacturer's guidelines. Transfection efficiency was monitored using a YFP-containing plasmid (pCW109, a kind gift from Dr Cheryl Walter). Transfected fibroblasts were collected two days and six days post-transfection. Immunocytochemistry, qRT-PCR and zymography was performed as described in the Supplementary Materials and Methods. HDF CM was profiled with a Proteome Profiler Human Cytokine Array Kit (R&D systems) following manufacturer's instructions.

Human Wound Repair. To assess the effects of CXCR2 blockade on human wound repair, analyses were performed on confluent monolayers of HaCaTs *in vitro*, and human wounds *ex vivo* as described in the Supplementary Materials and Methods.

Statistical Analysis. Data were shown as mean +/- standard deviations of the mean (SEM). Statistical tests (independent *t* tests, one-way ANOVA and two-way ANOVA) were performed on all quantitative data using GraphPad Prism 7 (GraphPad Software, California, US). Where applicable, *post-hoc* tests (Sidak, Dunnett's and Tukey) were performed. Differences between experimental groups were deemed significant when $P < 0.05$.

CONFLICT OF INTEREST

The authors state no conflict of interest.

ACKNOWLEDGEMENTS

An MRC (UK) CASE PhD Studentship supported this work (grant number: MR/M016307/1). We would like to thank Dr Cheryl Walter (Biomedical Sciences, The University of Hull) for sharing materials and advice.

AUTHOR CONTRIBUTIONS STATEMENT

The authors contributed in the following ways: study design and concept: HW, CC and MH; acquisition of data: HW and CC; analysis and interpretation of data: HW, CC, KB, KM and MH; drafting of the manuscript: HW and MH; critical revision of the manuscript: HW, KB, KM, PM and MH; acquisition of funding: MH; study supervision: MH.

REFERENCES

Acosta, J.C., O'Loghlen, A., Banito, A., Guijarro, M.V., Augert, A., Raguz, S., et al. **Chemokine signaling via the CXCR2 receptor reinforces senescence.** *Cell*. 2008; 133:1006-1018.

Ågren, M. S., Steenfos, H. H., Dabelsteen, S., Hansen, J. B., & Dabelsteen, E. **Proliferation and Mitogenic Response to PDGF-BB of Fibroblasts Isolated from Chronic Venous Leg Ulcers is Ulcer-Age Dependent1**. *J Invest Dermatol*. 1999; 112:463-469.

Ansell, D. M., Holden, K. A., Hardman, M. J. **Animal models of wound repair: Are they cutting it?** *Exp Dermatol*. 2012;21:581-585.

Ashcroft, G. S., Mills, S. J., Lei, K., Gibbons, L., Jeong, M.-J., Taniguchi, M., et al. **Estrogen modulates cutaneous wound healing by downregulating macrophage migration inhibitory factor**. *J Clin Invest.* 2003;111:1309-1318.

Baker, D. J., Childs, B. G., Durik, M., Wijers, M. E., Sieben, C. J., Zhong, J., et al. **Naturally occurring p16 Ink4a-positive cells shorten healthy lifespan.** *Nature.* 2016;530:184-189.

Baker, D. J., Perez-Terzic, C., Jin, F., Pitel, K. S., Niederländer, N. J., Jeganathan, K., et al. **Opposing roles for p16 Ink4a and p19 Arf in senescence and ageing caused by BubR1 insufficiency**. *Nat Cell Biol.* 2008;10:825-836.

Baker, D. J., Wijshake, T., Tchkonia, T., LeBrasseur, N. K., Childs, B. G., Van De Sluis, B., et al. **Clearance of p16Ink4a-positive senescent cells delays ageing-associated disorders**. *Nature*. 2011;479:232-236.

Balkwill, F. R. **The chemokine system and cancer.** *J Pathol*. 2012;226:148-157.

Bannon, P., Wood, S., Restivo, T., Campbell, L., Hardman, M. J., Mace, K. A. **Diabetes induces stable intrinsic changes to myeloid cells that contribute to chronic inflammation during wound healing in mice**. *Dis Mod Mech*. 2013;6:1434-1447.

Beauséjour, C. M., Krtolica, A., Galimi, F., Narita, M., Lowe, S. W., Yaswen, P., et al. **Reversal of human cellular senescence: roles of the p53 and p16 pathways.** *EMBO J.* 2003;22:4212-4222.

Berry, D. C., Jiang, Y., Arpke, R. W., Close, E. L., Uchida, A., Reading, D., et al. **Cellular aging contributes to failure of cold-induced beige adipocyte formation in old mice and humans**. *Cell Metab*. 2017;25:166-181.

Bradley, M. E., Bond, M. E., Manini, J., Brown, Z., Charlton, S. J. **SB265610 is an allosteric, inverse agonist at the human CXCR2 receptor.** *Br J Pharmacol*. 2009;158:328-338.

Campisi, J., di Fagagna, F. d. A. **Cellular senescence: when bad things happen to good cells.** *Nat Rev Mol Cell Biol*. 2007;8:729.

Campisi, J., Robert, L. **Cell senescence: role in aging and age-related diseases**. *Interdiscip Top Gerontol*. 2014;39:45-61.

Chien, Y., Scuoppo, C., Wang, X., Fang, X., Balgley, B., Bolden, J. E., et al. **Control of the senescence-associated secretory phenotype by NF-κB promotes senescence and enhances chemosensitivity**. *Genes Dev*. 2011;25:2125-2136.

Childs, B. G., Baker, D. J., Kirkland, J. L., Campisi, J., & Van Deursen, J. M. **Senescence and apoptosis: dueling or complementary cell fates?** *EMBO Reports*. 2014; 15:1139-1153.

Choudhury, A. R., Ju, Z., Djojosubroto, M. W., Schienke, A., Lechel, A., Schaetzlein, S., et al. **Cdkn1a deletion improves stem cell function and lifespan of mice with dysfunctional telomeres without accelerating cancer formation**. *Nat. Gen*. 2017;39: 99-105.

Coppé, J.-P., Desprez, P.-Y., Krtolica, A., Campisi, J. (2010). **The senescence-associated secretory phenotype: the dark side of tumor suppression**. *Annu Rev Pathol Mech Dis*. 2010;5:99-118.

Coppé, J.-P., Patil, C. K., Rodier, F., Sun, Y., Muñoz, D. P., Goldstein, J., et al. **Senescence-associated secretory phenotypes reveal cell-nonautonomous functions of oncogenic RAS and the p53 tumor suppressor.** *PLoS Biol*. 2008;6:e301.

Demaria, M., Ohtani, N., Youssef, S. A., Rodier, F., Toussaint, W., Mitchell, J. R., et al. **An essential role for senescent cells in optimal wound healing through secretion of PDGF-AA**. *Dev Cell*. 2014;31:722-733.

Devalaraja, R. M., Nanney, L. B., Qian, Q., Du, J., Yu, Y., Devalaraja, M. N., et al. **Delayed wound healing in CXCR2 knockout mice**. *J Invest Dermatol*. 2000;115: 234-244.

Di Micco, R., Fumagalli, M., Cicalese, A., Piccinin, S., Gasparini, P., Luise, C., et al. **Oncogene-induced senescence is a DNA damage response triggered by DNA hyper-replication.** *Nature*. 2006;444: 638-642.

Dimova, D. K., Dyson, N. J. **The E2F transcriptional network: old acquaintances with new faces.** *Oncogene*. 2005;24:2810-2826.

Erusalimsky, J. D., Kurz, D. J. **Cellular senescence in vivo: its relevance in ageing and cardiovascular disease.** *Exp. Geront*. 2005;40:634-642.

Freund, A., Orjalo, A. V., Desprez, P.-Y., Campisi, J. **Inflammatory networks during cellular senescence: causes and consequences.** *Trends Mol Med*. 2010;16:238-246.

Goova, M. T., Li, J., Kislinger, T., Qu, W., Lu, Y., Bucciarelli, L. G., et al. **Blockade of receptor for advanced glycation end-products restores effective wound healing in diabetic mice.** *Am J Pathol*. 2001;159:513-525.

Harding, K. G., Moore, K., Phillips, T. J. **Wound chronicity and fibroblast senescence–implications for treatment.** *Int Wound J*. 2005;2:364-368.

Hayflick, L., Moorhead, P. S. **The serial cultivation of human diploid cell strains.** *Exp Cell Res*. 1961;25:585-621.

He, L., He, X., Lim, L. P., De Stanchina, E., Xuan, Z., Liang, Y., et al. **A microRNA component of the p53 tumour suppressor network.** *Nature*. 2007;447:1130-1134.

Jun, J.-I., Lau, L. F. **The matricellular protein CCN1 induces fibroblast senescence and restricts fibrosis in cutaneous wound healing**. *Nat Cell Biol*. 2010;12:676-685.

Kamei, N., Tobe, K., Suzuki, R., Ohsugi, M., Watanabe, T., Kubota, N., et al. **Overexpression of monocyte chemoattractant protein-1 in adipose tissues causes macrophage recruitment and insulin resistance**. *J Biol Chem*. 2006;281:26602-26614.

Khanna, S., Biswas, S., Shang, Y., Collard, E., Azad, A., Kauh, C., et al. **Macrophage dysfunction impairs resolution of inflammation in the wounds of diabetic mice.** *PloS ONE*. 2010;5:e9539.

Kim, D. J., Mustoe, T., Clark, R. A. **Cutaneous wound healing in aging small mammals: a systematic review.** *Wound Rep Regen*. 2015;23:318-339.

Koh, T. J., DiPietro, L. A. **Inflammation and wound healing: the role of the macrophage.** *Expert Rev Mol Med*. 2011;13:e23.

Kortlever, R. M., Higgins, P. J., Bernards, R. **Plasminogen activator inhibitor-1 is a critical downstream target of p53 in the induction of replicative senescence**. *Nature Cell Biol*. 2006;8:877-884.

Krishnamurthy, J., Ramsey, M. R., Ligon, K. L., Torrice, C., Koh, A., Bonner-Weir, S., et al. **p16 INK4a induces an age-dependent decline in islet regenerative potential.** *Nature*, 2006;443:453-457.

Krizhanovsky, V., Yon, M., Dickins, R. A., Hearn, S., Simon, J., Miething, C., et al. **Senescence of activated stellate cells limits liver fibrosis.** Cell. 2008;134:657-667.

Kroeze, K. L., Boink, M. A., Sampat-Sardjoepersad, S. C., Waaijman, T., Scheper, R. J., Gibbs, S. **Autocrine regulation of re-epithelialization after wounding by chemokine receptors CCR1, CCR10, CXCR1, CXCR2, and CXCR3.** *J Invest Dermatol*. 2012;132:216-225.

Li, Y., Tollefsbol, T. O. **p16INK4a suppression by glucose restriction contributes to human cellular lifespan extension through SIRT1-mediated epigenetic and genetic mechanisms.** *PLoS ONE*. 2011;6:e17421.

Liu, J., Huang, K., Cai, G.-Y., Chen, X.-M., Yang, J.-R., Lin, L.-R., et al. **Receptor for advanced glycation end-products promotes premature senescence of proximal tubular epithelial cells via activation of endoplasmic reticulum stress-dependent p21 signaling.** *Cell* Signal. 2014;26:110-121.

Malumbres, M., Barbacid, M. **Mammalian cyclin-dependent kinases.** *Trends Biochem Sci*. 2005;30:630-641.

Mantovani, A., Biswas, S. K., Galdiero, M. R., Sica, A., Locati, M. **Macrophage plasticity and polarization in tissue repair and remodelling.** *J Pathol*. 2013;229:176-185.

Matthaei, M., Meng, H., Meeker, A.K., Eberhart, C.G., Jun, A.S. **Endothelial Cdkn1a (p21) overexpression and accelerated senescence in a mouse model of Fuchs endothelial corneal dystrophy.** *Invest Ophthalmol Vis Sci*. 2012;53:6718-6727.

*McCloy, R.A., Rogers, S., Caldon, C.E., Lorca, T., Castro, A., Burgess, A. **Partial inhibition of Cdk1 in G2 phase overrides the SAC and decouples mitotic events**. *Cell Cycle*. 2014;13:1400-1412.

Mendez, M. V., Stanley, A., Park, H. Y., Shon, K., Phillips, T., & Menzoian, J. O. **Fibroblasts cultured from venous ulcers display cellular characteristics of senescence**. *J Vasc Surg*. 1998;28:876-883.

Milatovic, S., Nanney, L. B., Yu, Y., White, J. R., Richmond, A. **Impaired healing of nitrogen mustard wounds in CXCR2 null mice.** *Wound repair and regeneration*. 2003;11:213-219.

Minamino, T., Orimo, M., Shimizu, I., Kunieda, T., Yokoyama, M., Ito, T., et al. A **crucial role for adipose tissue p53 in the regulation of insulin resistance**. *Nat Med*. 2009;15:1082-1087.

Mirza, R. E., Fang, M. M., Novak, M. L., Urao, N., Sui, A., Ennis, W. J., et al. **Macrophage PPARγ and impaired wound healing in type 2 diabetes**. *J Pathol*. 2015;236:433-444.

Moiseeva, O., Deschênes-Simard, X., St-Germain, E., Igelmann, S., Huot, G., Cadar, A. E., et al. **Metformin inhibits the senescence-associated secretory phenotype by interfering with IKK/NF-κB activation.** *Aging Cell*. 2013;*12*:489-498.

Müller, K. M., Bickel, M., Wiesmann, U. N., Spörri, B. **Natural killer cells activate human dermal fibroblasts.** *Cytokine*. 2000;12:1755-1762.

Naidoo, N., Brown, M. **The endoplasmic reticulum stress response in aging and age-related diseases**. *Front Physiol*. 2012;3:263.

Narita, M., Nuñez, S., Heard, E., Narita, M., Lin, A. W., Hearn, S. A., et al. **Rb-mediated heterochromatin formation and silencing of E2F target genes during cellular senescence**. *Cell*. 2003;113:703-716.

Nguyen T, Nioi P, Pickett CB. **The Nrf2-antioxidant response element signaling pathway and its activation by oxidative stress**. *J Biol Chem*. 2009;284:13291-13295.

Passos, J. F., Nelson, G., Wang, C., Richter, T., Simillion, C., Proctor, C. J., et al. **Feedback between p21 and reactive oxygen production is necessary for cell senescence.** *Mol Syst Biol.* 2010;6:347.

Peng, Y., Xuan, M., Leung, V.Y., Cheng, B. **Stem cells and aberrant signaling of molecular systems in skin aging**. *Ageing Res Rev*. 2015;19:8-21.

Prattichizzo, F., De Nigris, V., Mancuso, E., Spiga, R., Giuliani, A., Matacchione et al. **Short-term sustained hyperglycaemia fosters an archetypal senescence-associated secretory phenotype in endothelial cells and macrophages**. *Redox Biol*. 2018;15:170-181.

Rodier, F., Coppé, J.-P., Patil, C. K., Hoeijmakers, W. A., Muñoz, D. P., Raza, S. R., et al. **Persistent DNA damage signalling triggers senescence-associated inflammatory cytokine secretion**. *Nat Cell Biol*. 2009;11:973.

Sagiv, A., Krizhanovsky, V. **Immunosurveillance of senescent cells: the bright side of the senescence program.** *Biogerontology*. 2013;14: 17-628.

Satriano, J., Mansoury, H., Deng, A., Sharma, K., Vallon, V., Blantz, R. C., et al. **Transition of kidney tubule cells to a senescent phenotype in early experimental diabetes**. *Am J Physiol Cell Physiol*. 2010;299:C374-C380.

Schafer, M. J., White, T. A., Evans, G., Tonne, J. M., Verzosa, G. C., Stout, M. B., et al. **Exercise prevents diet-induced cellular senescence in adipose tissue.** *Diabetes*. 2016;65:1606-1615.

Sone, H., Kagawa, Y. **Pancreatic beta cell senescence contributes to the pathogenesis of type 2 diabetes in high-fat diet-induced diabetic mice**. *Diabetologia*. 2005;48:58-67.

Spranger, J., Kroke, A., Möhlig, M., Bergmann, M. M., Ristow, M., Boeing, H., et al. **Adiponectin and protection against type 2 diabetes mellitus**. *Lancet*. 2003;361:226-228.

Stanley, A., Osler, T. **Senescence and the healing rates of venous ulcers**. *J Vasc Surg*. 2001;33:1206-1211.

Stephens, P., Cook, H., Hilton, J., Jones, C. J., Haughton, M. F., Wyllie, F. S., et al. **An analysis of replicative senescence in dermal fibroblasts derived from chronic leg wounds predicts that telomerase therapy would fail to reverse their disease-specific cellular and proteolytic phenotype**. *Exp Cell Res*. 2003;283:22-35.

Storer, M., Mas, A., Robert-Moreno, A., Pecoraro, M., Ortells, M. C., Di Giacomo, V., et al. **Senescence is a developmental mechanism that contributes to embryonic growth and patterning**. *Cell*. 2013;155:1119-1130.

Takahashi, A., Ohtani, N., Yamakoshi, K., Iida, S.-i., Tahara, H., Nakayama, K., et al. **Mitogenic signalling and the p16 INK4a–Rb pathway cooperate to enforce irreversible cellular senescence**. *Nat Cell Biol*. 2006;8:1291.

Tchkonia, T., Zhu, Y., Van Deursen, J., Campisi, J., Kirkland, J. L. **Cellular senescence and the senescent secretory phenotype: therapeutic opportunities**. *J Invest Dermatol*. 2013;123:966-972.

Vande Berg, J. S., Rudolph, R., Hollan, C., & Haywood‐Reid, P. L. **Fibroblast senescence in pressure ulcers**. *Wound Rep Regen*. 1998;6:38-49.

*Weischenfeldt, J., Porse, B. **Bone marrow-derived macrophages (BMM): isolation and applications**. *Cold Spring Harb Protoc*. 2008; **12**:pdb-rot5080.

Wetzler, C., Kämpfer, H., Stallmeyer, B., Pfeilschifter, J., Frank, S. **Large and sustained induction of chemokines during impaired wound healing in the genetically diabetic mouse: prolonged persistence of neutrophils and macrophages during the late phase of repair**. *J Invest Dermatol.* 2000;115:245-253.

Wilkinson, H.N., Iveson, S., Catherall, P., Hardman, M.J. **A Novel Silver Bioactive Glass Elicits Antimicrobial Efficacy Against Pseudomonas aeruginosa and Staphylococcus aureus in an ex Vivo Skin Wound Biofilm Model**. *Front Microbiol*. 2018;9:1450.

Wood, S., Jayaraman, V., Huelsmann, E.J., Bonish, B., Burgad, D., Sivaramakrishnan, et al., **Pro-inflammatory chemokine CCL2 (MCP-1) promotes healing in diabetic wounds by restoring the macrophage response**. *PLoS ONE.* 2014;9:e91574.

Xu, H., Barnes, G.T., Yang, Q., Tan, G., Yang, D., Chou, C.J., et al. **Chronic inflammation in fat plays a crucial role in the development of obesity-related insulin resistance**. *J Clin Invest.* 2003;112:1821-1830.

Yosef, R., Pilpel, N., Papismadov, N., Gal, H., Ovadya, Y., Vadai, E., et al. **p21 maintains senescent cell viability under persistent DNA damage response by restraining JNK and caspase signaling.** *EMBO J*. 2017;37:e201695553.

*Cited only in Supplementary Material.

FIGURE LEGENDS

Figure 1. SA-βGAL staining elucidates pathological accumulation of senescent cells in murine skin and wounds. Here, senescence-associated beta galactosidase (SA-βGAL) staining illustrated increased senescent dermal cells in aged skin and diabetic (Db) and aged wounds (**a**, compared to young). Representative images of SA-βGAL+ve (blue) cells are shown in **b**, depicted by black arrows (n=5-6 per group). Bars = 100 μm. Further profiling of senescence markers via qRT-PCR demonstrated an increase in *Cdkn1a* (**c**), *Cdkn1b* (**d**), *Cdkn2a* (**e**) and *Trp53* (**f**) in aged skin, while *Cdkn1a* was only upregulated in Db wounds. D0 = normal skin. D7 = day 7 post-injury wounds. n=3-4 per group. Data represent mean +/- SEM. * = $P < 0.05$, ** = $P < 0.01$, *** = $P < 0.001$.

Figure 2. Diabetic wounds show heightened recruitment of macrophages, which are intrinsically susceptible to senescence. Masson's Trichrome staining comparing diabetic (Db) and non-diabetic (NDb) wounds (**a**; quantified in **b**) at day 7 post-injury. Wound edges = black arrows. Bar = 500 μm. Db wounds contain highly senescent macrophages (Mφs; **c**), demonstrated via representative immunofluorescence (**d**, white arrows). Bar = 20 μm. n=4-6 mice per group. Bone marrow-derived Db Mφs demonstrated significantly more SA-βGAL+ve staining (**e**; blue cells, **f**). Bar = 50 μm. Polarised Db Mφs possessed heightened *Cdkn1a* and *Cdkn2a* mRNA 72 hours post-cytokine stimulation with less *Nos2* and *Ym1* than NDb Mφs (**g**). Immunofluorescence further demonstrates reduced polarisation of Db Mφs (merged images, **h**). Bar = 20 μm. n=5 animals per group. Data show mean +/- SEM. * = $P < 0.05$, ** = $P < 0.01$, *** = $P < 0.001$.

Figure 3. Diabetic macrophages produce a SASP governed by the CXCR2 receptor that alters human dermal fibroblast gene expression. Cytokine array of conditioned media (CM) from M1 and M2 non-diabetic (NDb) and diabetic (Db) macrophages (Mφs; **a-b**; two independent experiments; representative M2 blots). CXCL1 = not expressed in NDb M2 Mφs

(∞). qRT-PCR of *Cxcl1*, *Cxcl2* and *Cxcr2* in Db Mφs (**c**). Zymography of Mφ CM protease (quantified in **d**). qRT-PCR for *Cxcl1* (**e**), *Cxcl2* (**f**) and *Cxcr2* (**g**), performed on skin (D0) and wounds (D7) from mice. Mφ CM stimulated changes in human dermal fibroblast gene expression (Db versus NDb fold changes, **h**). n=3 human donors per group. Fold changes above 4 and below -4 = saturated colour. Data show mean +/- SEM. * = $P < 0.05$, ** = $P < 0.01$, *** = $P < 0.001$.

Figure 4. Ectopic expression of CXCL2 induces paracrine activity that influences nuclear localisation of p21. Human dermal fibroblasts transfected with a CXCL2-containing plasmid show heightened levels of CXCL2 (green fluorescence) at day 2 (D2) post-transfection, that are further upregulated by D6 (**a**, quantified in **b**). CXCL2-transfected fibroblasts also displayed elevated nuclear p21 (red fluorescence) by D6 post-transfection (**c-d**). DAPI = nuclei. CTCF = corrected total cell fluorescence. Bar = 50 µm. YFP-positive staining (**e**). CXCL2 expressing HDFs also produced a SASP-rich secretome (blot, **f**, graph, **g**), while zymography shows changes in MMP2 activity (**h**, representative of 3 gels, quantification in **i**). qRT-PCR demonstrated changes in *MMP2*, *COL3A1* and *COL1A1* between control-transfected and CXCL2-transfected HDFs (**j**). Data = mean +/- SEM. * = $P < 0.05$, *** = $P < 0.001$.

Figure 5. Early phase wound repair is accelerated by blockade of CXCR2 in human *ex vivo* healing. K14 staining (**a** and **c**) demonstrated a significant increase in epidermal wound closure after 3 days following treatment of human *ex vivo* wounds with the CXCR2 antagonist, SB265610 (**E**; arrows show wound edges, bar = 200 µm), whereas combined treatment with CXCL1 and CXCL2 delayed healing (**D**). Combining SB265610 with CXCL2 (**G**), but not CXCL1 (**F**), rescued the delay in wound healing, but SB265610 did not rescue healing with combinatory ligand treatment (**H**). Letters in **a** and **b** relate to treatments in **c** and **d**. K6 staining (**b**; bar = 50 µm), depicted increased neo-epidermal proliferation following SB265610

treatment (**d**). Dotted lines = neo-epidermis. n=3 donors per treatment. Data show mean +/- SEM. * = $P < 0.05$, ** = $P < 0.01$.

Figure 6. Blocking CXCR2 significantly improves diabetic wound healing *in vivo*. Haematoxylin and eosin (**a**) staining showed significantly reduced wound width (**b**) and area (**c**) following SB265610 treatment (arrows show wound edges, bar = 500 μm). Immune cell infiltration was dampened, quantified from neutrophil (**d**) and macrophage (**e**) staining. Macrophage (Mac3) senescence (p16+ve macrophages) was also reduced following SB265610 treatment (**f**). DAPI = nuclei; Alexa Fluor® 488 = Mac3; Alexa Fluor® 647 = p16. Representative images (**g** and **h**). Bar = 50 μm. Wounds collected at day 7 post-injury. Arrows show positively stained cells. Data show mean +/- SEM. * = $P < 0.05$, ** = $P < 0.01$, *** = $P < 0.001$.

SUPPLEMENTARY MATERIAL

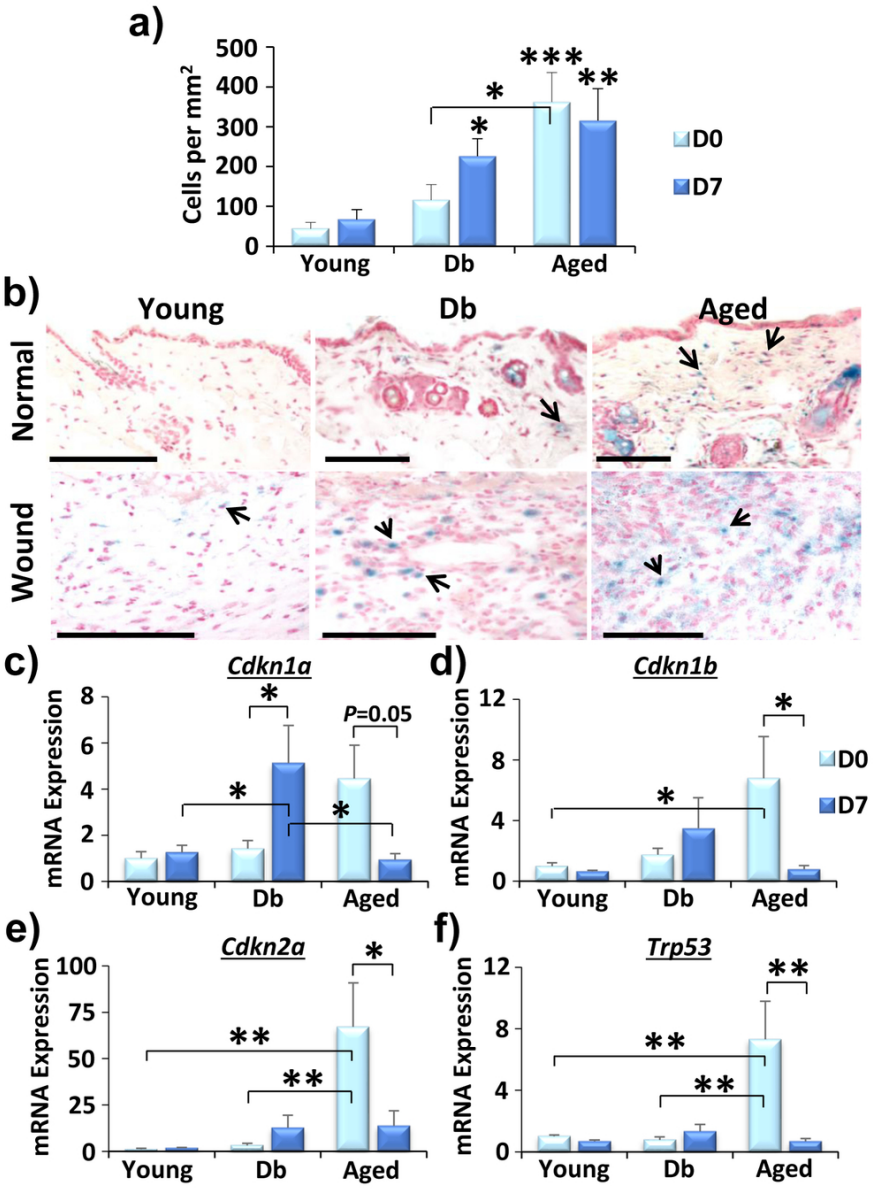

Figure 1. SA-βGAL staining elucidates pathological accumulation of senescent cells in murine skin and wounds. Here, senescence-associated beta galactosidase (SA-βGAL) staining illustrated increased senescent dermal cells in aged skin and diabetic (Db) and aged wounds (**a**, compared to young). Representative images of SA-βGAL+ve (blue) cells are shown in **b**, depicted by black arrows (n=5-6 per group). Bars = 100 μm. Further profiling of senescence markers via qRT-PCR demonstrated an increase in *Cdkn1a* (**c**), *Cdkn1b* (**d**), *Cdkn2a* (**e**) and *Trp53* (**f**) in aged skin, while *Cdkn1a* was only upregulated in Db wounds. D0 = normal skin. D7 = day 7 post-injury wounds. n=3-4 per group. Data represent mean +/- SEM. * = $P < 0.05$, ** = $P < 0.01$, *** = $P < 0.001$.

83x114mm (300 x 300 DPI)

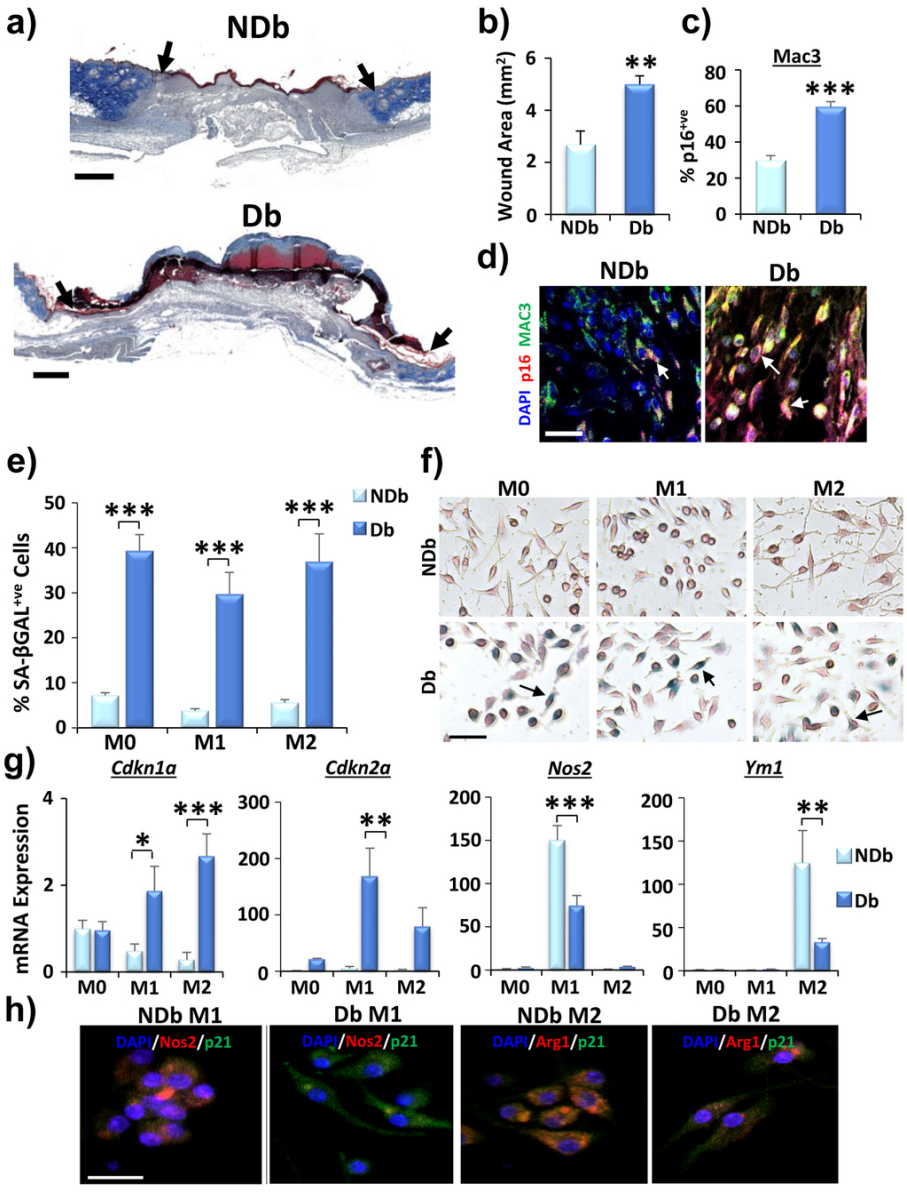

Figure 2. Diabetic wounds show heightened recruitment of macrophages, which are intrinsically susceptible to senescence. Masson's Trichrome staining comparing diabetic (Db) and non-diabetic (NDb) wounds (**a**; quantified in **b**) at day 7 post-injury. Wound edges = black arrows. Bar = 500 μm. Db wounds contain highly senescent macrophages (Mφs; **c**), demonstrated via representative immunofluorescence (**d**, white arrows). Bar = 20 μm. n=4-6 mice per group. Bone marrow-derived Db Mφs demonstrated significantly more SA-βGAL+ve staining (**e**; blue cells, **f**). Bar = 50 μm. Polarised Db Mφs possessed heightened *Cdkn1a* and *Cdkn2a* mRNA 72 hours post-cytokine stimulation with less *Nos2* and *Ym1* than NDb Mφs (**g**). Immunofluorescence further demonstrates reduced polarisation of Db Mφs (merged images, **h**). Bar = 20 μm. n=5 animals per group. Data show mean +/- SEM. * = $P < 0.05$, ** = $P < 0.01$, *** = $P < 0.001$.

87x114mm (300 x 300 DPI)

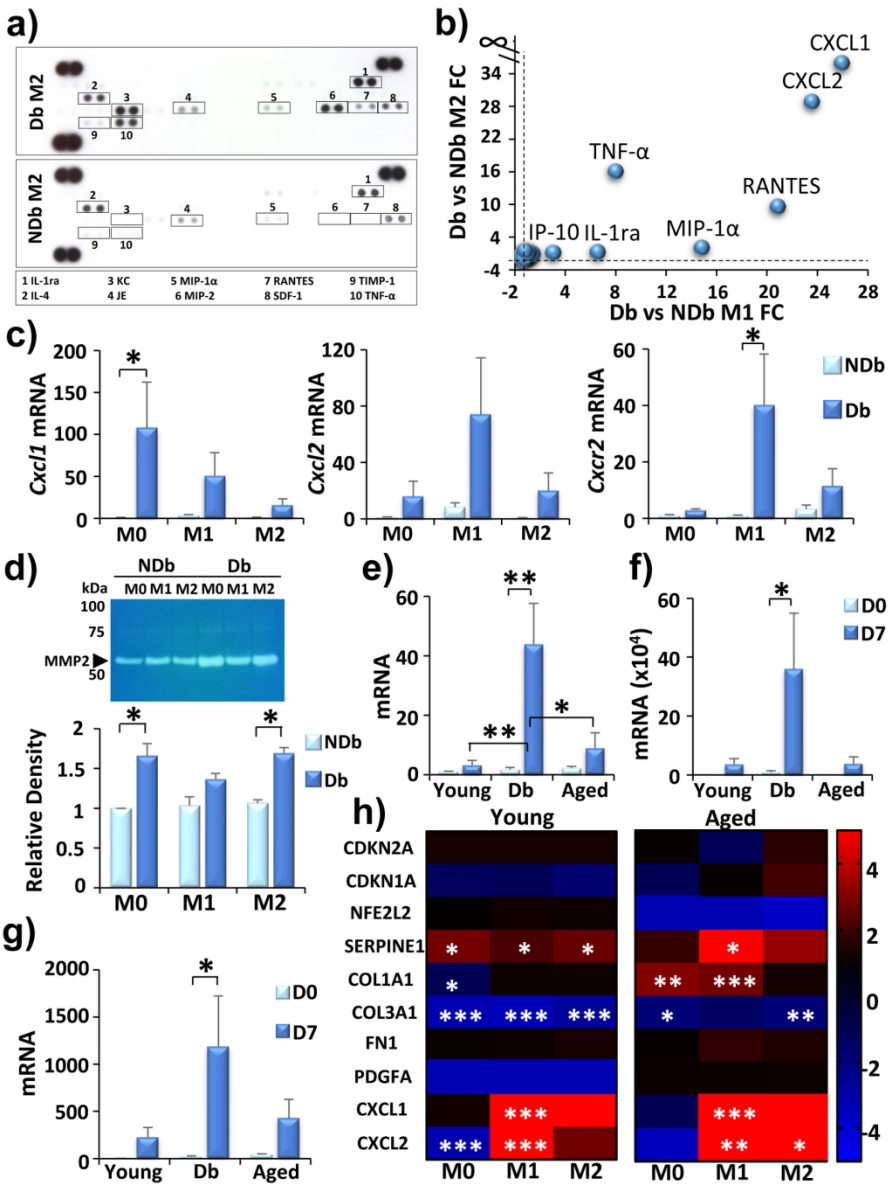

Figure 3. Diabetic macrophages produce a SASP governed by the CXCR2 receptor that alters human dermal fibroblast gene expression. Cytokine array of conditioned media (CM) from M1 and M2 non-diabetic (NDb) and diabetic (Db) macrophages (Mφs; **a-b**; two independent experiments; representative M2 blots). CXCL1 = not expressed in NDb M2 Mφs (∞). qRT-PCR of *Cxcl1*, *Cxcl2* and *Cxcr2* in Db Mφs (**c**). Zymography of Mφ CM protease (quantified in **d**). qRT-PCR for *Cxcl1* (**e**), *Cxcl2* (**f**) and *Cxcr2* (**g**), performed on skin (D0) and wounds (D7) from mice. Mφ CM stimulated changes in human dermal fibroblast gene expression (Db versus NDb fold changes, **h**). n=3 human donors per group. Fold changes above 4 and below -4 = saturated colour. Data show mean +/- SEM. * = $P < 0.05$, ** = $P < 0.01$, *** = $P < 0.001$.

74x99mm (600 x 600 DPI)

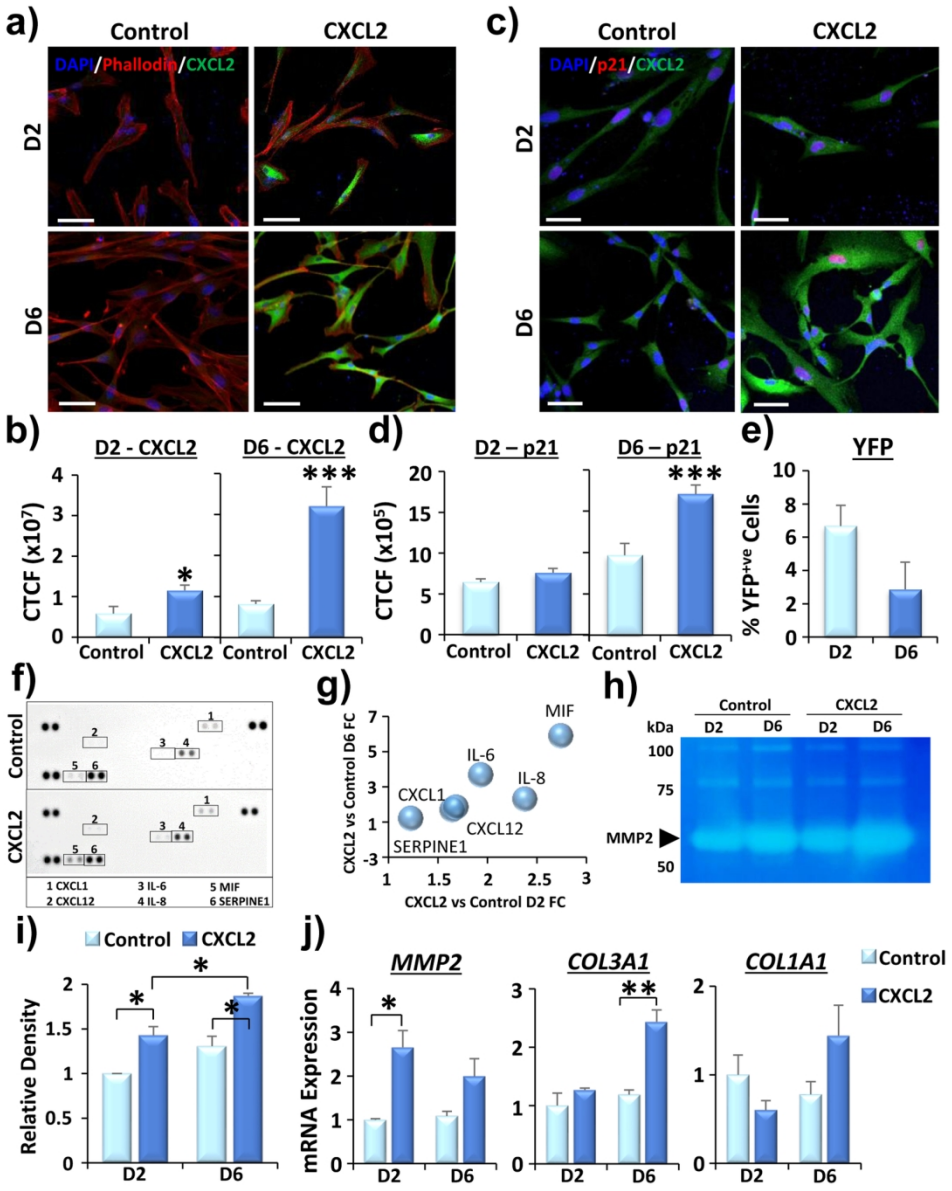

Figure 4. Ectopic expression of CXCL2 induces paracrine activity that influences nuclear localisation of p21. Human dermal fibroblasts transfected with a CXCL2-containing plasmid show heightened levels of CXCL2 (green fluorescence) at day 2 (D2) post-transfection, that are further upregulated by D6 (**a**, quantified in **b**). CXCL2-transfected fibroblasts also displayed elevated nuclear p21 (red fluorescence) by D6 post-transfection (**c-d**). DAPI = nuclei. CTCF = corrected total cell fluorescence. Bar = 50 µm. YFP-positive staining (**e**). CXCL2 expressing HDFs also produced a SASP-rich secretome (blot, **f**, graph, **g**), while zymography shows changes in MMP2 activity (**h**, representative of 3 gels, quantification in **i**). qRT-PCR demonstrated changes in *MMP2*, *COL3A1* and *COL1A1* between control-transfected and CXCL2-transfected HDFs (j). Data = mean +/- SEM. * = $P < 0.05$, *** = $P < 0.001$.

74x94mm (600 x 600 DPI)

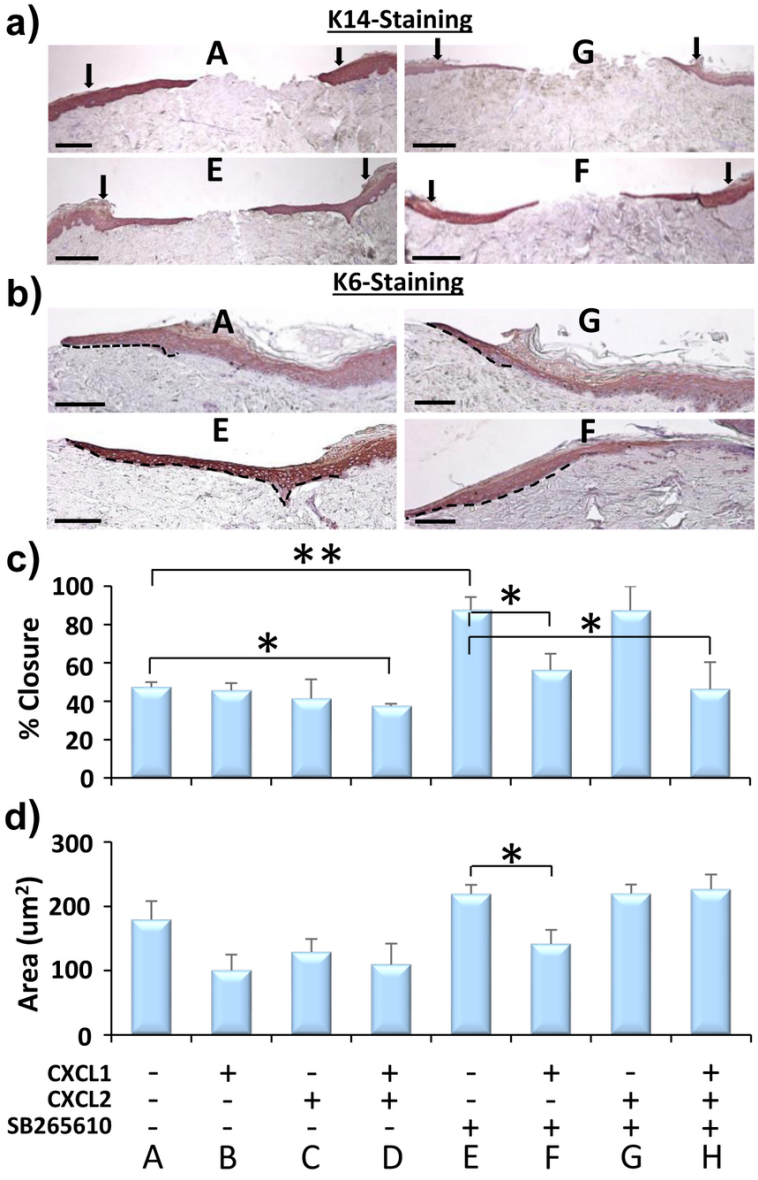

Figure 5. Early phase wound repair is accelerated by blockade of CXCR2 in human *ex vivo* healing. K14 staining (**a** and **c**) demonstrated a significant increase in epidermal wound closure after 3 days following treatment of human *ex vivo* wounds with the CXCR2 antagonist, SB265610 (E; arrows show wound edges, bar = 200 μm), whereas combined treatment with CXCL1 and CXCL2 delayed healing (D). Combining SB265610 with CXCL2 (G), but not CXCL1 (F), rescued the delay in wound healing, but SB265610 did not rescue healing with combinatory ligand treatment (H). Letters in **a** and **b** relate to treatments in **c** and **d**. K6 staining (**b**; bar = 50 μm), depicted increased neo-epidermal proliferation following SB265610 treatment (**d**). Dotted lines = neo-epidermis. n=3 donors per treatment. Data show mean +/- SEM. * = $P < 0.05$, ** = $P < 0.01$.

74x114mm (300 x 300 DPI)

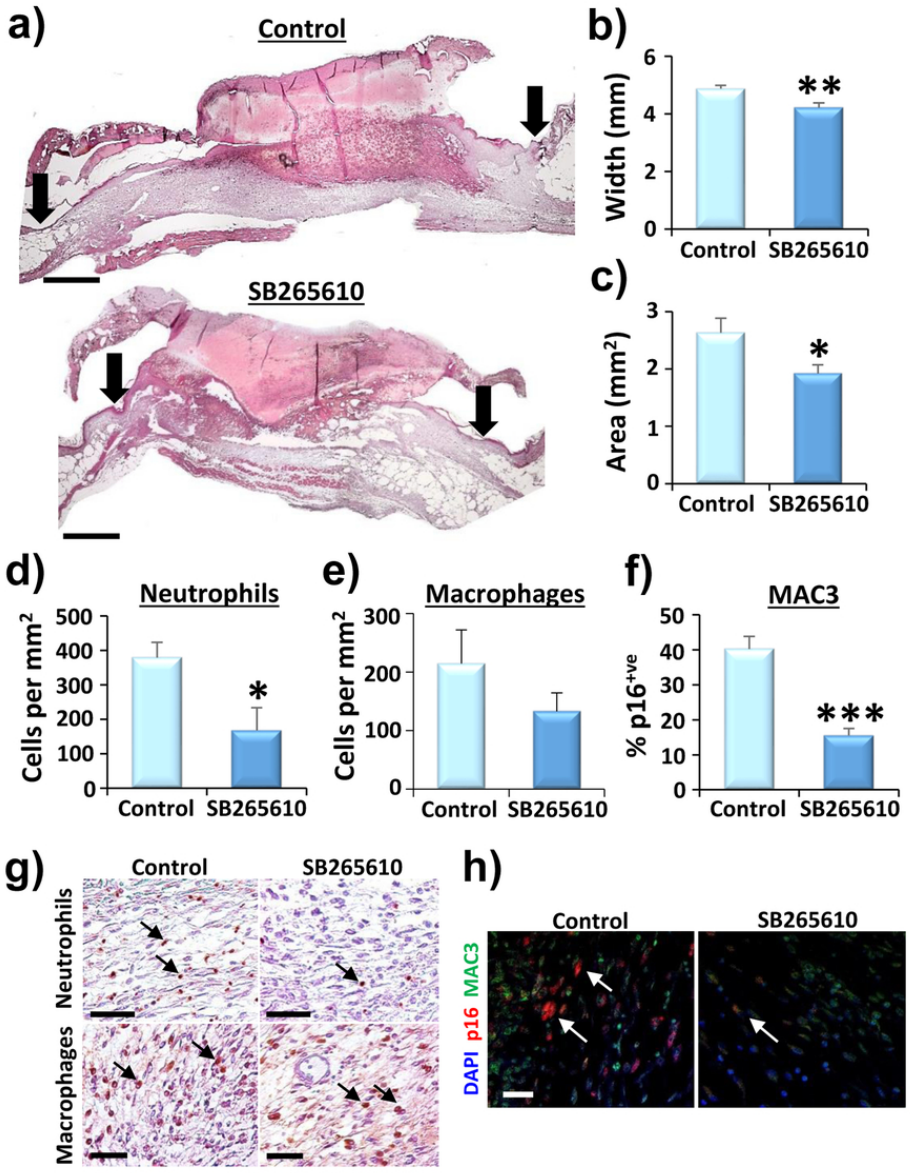

Figure 6. Blocking CXCR2 significantly improves diabetic wound healing *in vivo*. Haematoxylin and eosin (**a**) staining showed significantly reduced wound width (**b**) and area (**c**) following SB265610 treatment (arrows show wound edges, bar = 500 μm). Immune cell infiltration was dampened, quantified from neutrophil (**d**) and macrophage (**e**) staining. Macrophage (Mac3) senescence (p16+ve macrophages) was also reduced following SB265610 treatment (**f**). DAPI = nuclei; Alexa Fluor® 488 = Mac3; Alexa Fluor® 647 = p16. Representative images (**g** and **h**). Bar = 50 μm. Wounds collected at day 7 post-injury. Arrows show positively stained cells. Data show mean +/- SEM. * = $P < 0.05$, ** = $P < 0.01$, *** = $P < 0.001$.

74x96mm (300 x 300 DPI)

SUPPLEMENTARY TEXT

Supplementary Materials and Methods:

Tissue collection. Skin and wound tissue was collected from mice 7 days post-injury. Wounds were bisected at their midpoint and: a) placed in neutral buffered formalin for wax histology; b) flash frozen in liquid nitrogen and stored at -80 ºC for RNA analysis; and c) embedded in optimum cutting temperature medium (OCT) for SA-βGAL staining.

Histological analysis. Masson's trichrome staining and haematoxylin and eosin staining was performed on wax-embedded tissue sections (5 μm thick). Immunohistochemistry used rat anti-Ly-6G/Ly-6C (Clone NIMP-R14; Thermo Fisher Scientific, Paisley, UK), rat anti-Mac-3 (Clone M3/84; BD Biosciences, Reading, UK), goat anti-vimentin (VIM; Sigma-Aldrich, Dorset, UK), rabbit anti-p16 (Clone H-43; Santa Cruz Biotechnology, Heidelberg, Germany), rabbit anti-keratin 6A (Clone Poly19057) and rabbit anti-keratin 14 (Clone Poly19053; both Covance, London, UK) primary antibodies. For brightfield microscopy, appropriate biotinylated secondary antibody and VECTASTAIN® elite ABC kit were used with NovaRED™ peroxidase substrate (Vector Laboratories, Peterborough, UK). Tissue was counterstained with Gill's haematoxylin (Thermo Fisher Scientific, Paisley, UK). All brightfield images were taken with a Nikon E400 microscope and SPOT camera (Image Solutions, Inc. Michigan, US). Wound measurements were analysed in ImagePro-Plus v.6.3.0 (Media cybernetics, Cambridge, UK). For immunofluorescence, appropriate Alexa Fluor®-conjugated secondary antibodies were used (Alexa Fluor® 488 – Mac3; Alexa Fluor® 594 and 647 – p16; Thermo Fisher Scientific) and slides mounted with MOWIOL 488 (Sigma-Aldrich) containing DAPI (Thermo Fisher Scientific). Images were taken on a confocal laser scanning microscope (LSM 710, Zeiss) equipped with a 20x objective lens (Carl Zeiss Ltd., Cambridge, UK). DAPI, Alexa Fluor® 488, Alexa Fluor® 594 and Alexa Fluor® 647 were excited using

the 405 nm diode, 488 nm argon, 561 nm and 633 nm DPSS lasers, respectively. Pinhole size was equalled between lasers for optimum confocality. Mac3+ve and p16+ve cells were counted using ImageJ v.1.8.0.

qRT-PCR. RNA was extracted via homogenisation (tissue) or vortexing (cells) in Ambion™ TRIzol® reagent (Thermo Fisher Scientific). The aqueous phase was purified with the Ambion™ PureLink™ Mini Kit (Thermo Fisher Scientific). RNA purity and concentration was assessed with a Nanodrop spectrophotometer and adjusted to 1 µg/10 µl RNAse free water for cDNA synthesis. RNA was reverse transcribed with Bioscript™ (Bioline, London, UK) and random primers (Promega, Southampton, UK). The cDNA was diluted over three orders of magnitude and amplified with 2X Takyon SYBR Mastermix (Eurogentec, Hampshire, UK) and optimised primer sets on a CFX Connect™ qRT-PCR machine (Bio-Rad Laboratories, Hertfordshire, UK). Expression ratios of each gene were normalised to two housekeeping genes. Primer sequences are provided in **Supporting Information Table 1**.

Macrophage culture. Mononuclear phagocyte progenitor cells (from murine bone marrow) were cultured in low (NDb; LG; 1000 mg/L) or high (Db; HG; 4500 mg/L) glucose Dulbecco's Modified Essential Medium (DMEM, Sigma-Aldrich) with 10 % heat-inactivated foetal bovine serum (FBS, Thermo Fisher Scientific), 100 U/ml penicillin and 100 µg/ml streptomycin (P/S solution; Thermo Fisher Scientific). Differentiation (via M-CSF and other cytokines) of the progenitor cells into Mφs was propagated with L929 cell (NCTC clone 929, ATCC® CCL-1™) conditioned media (CM; as in Weischenfeldt et al., 2008).

Macrophage immunocytochemistry. Macrophages (Mφs), seeded on coverslips, were fixed with ice-cold methanol and probed for immunocytochemistry using the following antibodies: mouse anti-Nos2 (clone C-11), mouse anti-Arg1 (clone E-2), rabbit anti-p16 (above) and rat anti-p21 (clone HUGO291; Abcam, Cambridge, UK). Appropriate Alexa Fluor®-conjugated

secondary antibodies were used (Alexa Fluor® 488 – p16 and p21; Alexa Fluor® 594 – Nos2 and Arg1; Thermo Fisher Scientific) and coverslips mounted with MOWIOL 488 (Sigma-Aldrich) containing DAPI (Thermo Fisher Scientific). Images were taken on a confocal laser scanning microscope as described above.

Human fibroblast isolation. Human skin was collected under full ethical approval and informed consent from patients undergoing routine surgeries at Castle Hill Hospital, Cottingham, Hull (LREC 17/SC/0220). The subcutaneous adipose tissue was removed, and the skin was incubated in 0.2 % Dispase I (Thermo Fisher Scientific) O/N at 4 ºC. The following day, the epidermis and dermis were separated and human dermal fibroblasts (HDFs) isolated from the dermis using the Whole Skin Dissociation Kit skin and gentleMACS™ Dissociator (both Miltenyi Biotec Ltd, Woking, UK) following manufacturer's instructions. HDFs were cultured in standard Gibco HG DMEM containing 10 % FBS and 1 % P/S solution (Thermo Fisher Scientific).

Transfection experiments. Following transfection, immunocytochemistry of HDFs was performed with mouse anti-p21 (clone F5), rabbit anti-p16 (above; both Santa Cruz Biotechnology) and goat anti-CXCL2 (ab91511; Abcam) antibodies. Antibody-antigen binding was detected with Alexa Fluor® 488 and 594-conjugated secondary antibodies (Thermo Fisher Scientific) and the cytoskeleton was counterstained with Rhodamine-conjugated phallodin (Thermo Fisher Scientific) where shown. Coverslips were mounted with MOWIOL 488 (Sigma-Aldrich) containing DAPI (Thermo Fisher Scientific) and images captured via confocal laser scanning microscope (described above). Corrected total cell fluorescence (CTCF) was determined using ImageJ v.1.8 (NIH; as in McCloy et al., 2014), to compare CXCL2, p21 and p16 expression in MCS (pUNO1) and CXCL2 (pUNO1) transfected groups. YFP+ve cells were also counted using ImageJ v.1.8.0.

Scratch analysis. Confluent monolayers of HaCaTs (purchased from AddexBio, San Diego, US) were scratched with a sterile 1ml filter tip and treated with a vehicle (BSA/DMSO) or the CXCR2 ligands, CXCL1 and CXCL2 (30 ng/ml; R&D systems) alone and in combination. HaCaTs were also treated with a CXCR2 antagonist (100 nM, SB265610; R&D systems) alone or in combination with the ligands for 24 hours. Scratches, stained with 1 % crystal violet, were imaged (Nikon E400 microscope) and analysed in ImageJ V.1.8.0 (NIH).

Human ex vivo wounding. Human skin was washed in 2X antibiotic-antimycotic solution (Thermo Fisher Scientific) and defatted prior to wounding. Partial thickness (2 mm) wounds were created within 6 mm biopsies (using Stiefel biopsy punches, Stiefel Laboratories, NC, US). Wounds were placed on top of a sterile 0.22 µm membrane at the air-membrane interface on two absorbent pads (both Merck, Hertfordshire, UK) in 5mm petri dishes. HG DMEM, containing 10% FBS and 1% antibiotic-antimycotic solution, was added to the bottom of the dish. Treatments (described for scratch assays) were applied topically and re-administered daily. After 72 hours, samples were fixed (above) and epidermal repair was assessed via K6 and K14 histology (see above).

Supplementary Figure Legends:

Supplementary Figure S1. Aged skin and wounds possess high levels of p16. Immunohistochemistry or p16 staining in normal skin (D0) and wounds at day 7 post-injury (D7; **a**) from young, diabetic (Db) and aged mice. Representative images (**b**) show p16+ve cells (brown, black arrow). Bar = 50 µm. Data show mean +/- SEM. * = $P < 0.05$, ** = $P < 0.01$.

Supplementary Figure S2. Original zymography gel from Figure 3. Lane 1: Molecular weight ladder; Lane 3: Non-diabetic (NDb) M0 CM (conditioned media); Lane 4: NDb M1 CM; Lane 5: NDb M2 CM; Lane 6: Diabetic (Db) M0 CM; Lane 7: Db M1 CM; and Lane 8: Db M2 CM.

Supplementary Figure S3. Ectopic expression of CXCL2 drives upregulation of senescent markers in human fibroblasts. CXCL2-transfected fibroblasts show increased p16 (red; nuclei, blue) at D6 (day 6) post-transfection (**a-b**). Bar = 50 μm. CTCF = corrected total cell fluorescence. SA-βGAL staining is also increased in CXCL2-transfected fibroblasts at D2 and D6 (**c-d**). Bar = 100 μm. Data show mean +/- SEM. *** = $P < 0.001$.

Supplementary Figure S4. Original zymography gel from Figure 4. Lane 1: Molecular weight ladder; Lane 2: MMP2 standard. Lane 4: Control Day 2 CM (conditioned media); Lane 5: Control Day 6 CM; Lane 6: CXCL2 Day 2 CM; Lane 7: CXCL2 Day 6 CM.

Supplementary Figure S5. CXCR2 inhibition promotes HaCaT scratch migration after 24 hours treatment. The CXCR2 ligands, CXCL1 (A) and CXCL2 (B), impaired *in vitro* HaCaT wound closure (**b**), while treatment with the CXCR2 antagonist, SB265610 (E), accelerated scratch closure (representative of 3 independent experiments). Further, treatment with CXCL1 (F) and CXCL2 (G) with SB265610 independently did not delay scratch closure, whereas SB265610 failed to improve HaCaT migration when both ligands were combined (H). Crystal Violet-stained scratches are presented in **a**. Letters in **a** relate to treatments in **b**. Bar = 250 μm. * = $P < 0.05$, ** = $P < 0.01$, *** = $P < 0.001$.

Supplementary Figure S6. Complete representative images for human *ex vivo* wounding experiments. Keratin 14 (K14) and keratin 6 (K6) images of *ex vivo* wounds treated with a vehicle (**A**), CXCR2 ligands (CXCL1 and CXCL2) or the CXCR2 antagonist, SB265610 (alone, **E**). Wounds were also treated with combinations of the CXCR2 ligands and SB265610. The panel below the images explains the treatment groups labelled A-H. Arrows depict wound edges (K14). Dotted lines depict neo-epidermis (K6). K14 Bars = 200 μm. K6 Bars = 50 μm. Images representative of 3 human donors.

Supplementary Table S1. Primer sequences used for RT-qPCR*#

Primer	Forward Sequence	Reverse Sequence
mGapdh	TGCACCACCAACTGCTTAGC	GGCATGGACTGTGGTCATGAG
m18s	AGTCCCTGCCTTTGTACACA	CATCCGAGGGCCTAACTAAC
mYm1	GGCTACACTGGAGAAAATAGTCCCC	CCAACCCACTCATTACCCTGATAG
mNos2	GTGGTGACAAGCACATTTGG	AAGGCCAAACACAGCATACC
mCdkn1a (p21)#	CAGTACTTCCTCTGCCCTGC	GCTCAGACACCAGAGTGCAA
mCdkn1b (p27)	TTGGGTCTCAGGCAAACTCT	TTCTGTTCTGTTGGCCCTTT
mCdkn2a (p16)	GTACCCCGATTCAGGTGATG	CAGTTCGAATCTGCACCGTA
mTrp53 (p53)	AGAGACCGCCGTACAGAAGA	CTGTAGCATGGGCATCCTTT
mCxcl1	GCTGGGATTCACCTCAAGAA	TGGGGACACCTTTTAGCATC
mCxcl2	AGTGAACTGCGCTGTCAATG	TTCAGGGTCAAGGCAAACTT
mCxcr2	ATCTTCGCTGTCGTCCTTGT	AGCCAAGAATCTCCGTAGCA
hGAPDH	TGCACCACCAACTGCTTAGC	GGCATGGACTGTGGTCATGAG
hYWHAZ	ACTTTTGGTACATTGTGGCTTCAA	CCGCCAGGACAAACCAGTAT
hSERPINE1 (PAI-1)	ATACTGAGTTCACCACGCCC	GTTGGTGAGGGCAGAGAGAG
hCDKN1A	GACTCTCAGGGTCGAAAACG	CTCTTGGAGAAGATCAGCCG
hCDKN2A	GAGCAGCATGGAGCCTTC	CCGTAACTATTCGGTGCGTT
hCXCL2	GCAGGGAATTCACCTCAAGA	GGATTTGCCATTTTTCAGCA
hCXCL1	ATTCACCCCAAGAACATCCA	TGGATTTGTCACTGTTCAGCA

hCOL1A1	CACACGTCTCGGTCATGGTA	CGGCTCCTGCTCCTCTTAG
hCOL3A1	ATATTTGGCATGGTTCTGGC	TGGCTACTTCTCGCTCTGCT
hFN1	TGACCCCTACACAGTTTCCCA	TGATTCAGACATTCGTTCCCAC
hNFE2L2 (NRF2)	AAACCAGTGGATCTGCCAAC	ACGTAGCCGAAGAAACCTCA
hPDGFA	ACACGAGCAGTGTCAAGTGC	CCTGACGTATTCCACCTTGG
hMMP2	ATGACAGCTGCACCACTGAG	ATTTGTTGCCCAGGAAAGTG

*Housekeeping genes: mGapdh and m18s (mouse) and hGAPDH and hYWHAZ (human).

#Encoded protein is provided in brackets if this differed from gene nomenclature.

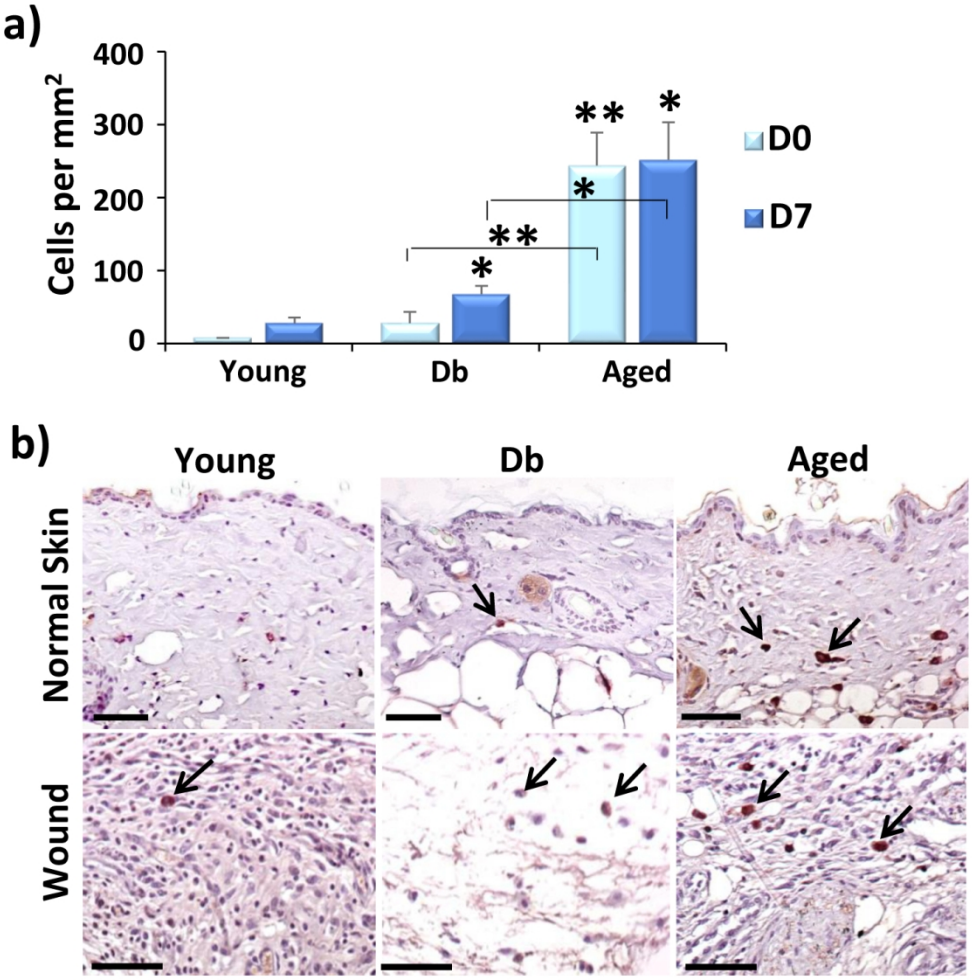

Supplementary Figure S1. Aged skin and wounds possess high levels of p16. Immunohistochemistry or p16 staining in normal skin (D0) and wounds at day 7 post-injury (D7; **a**) from young, diabetic (Db) and aged mice. Representative images (**b**) show p16+ve cells (brown, black arrow). Bar = 50 μm. Data show mean +/- SEM. * = $P < 0.05$, ** = $P < 0.01$.

127x130mm (300 x 300 DPI)

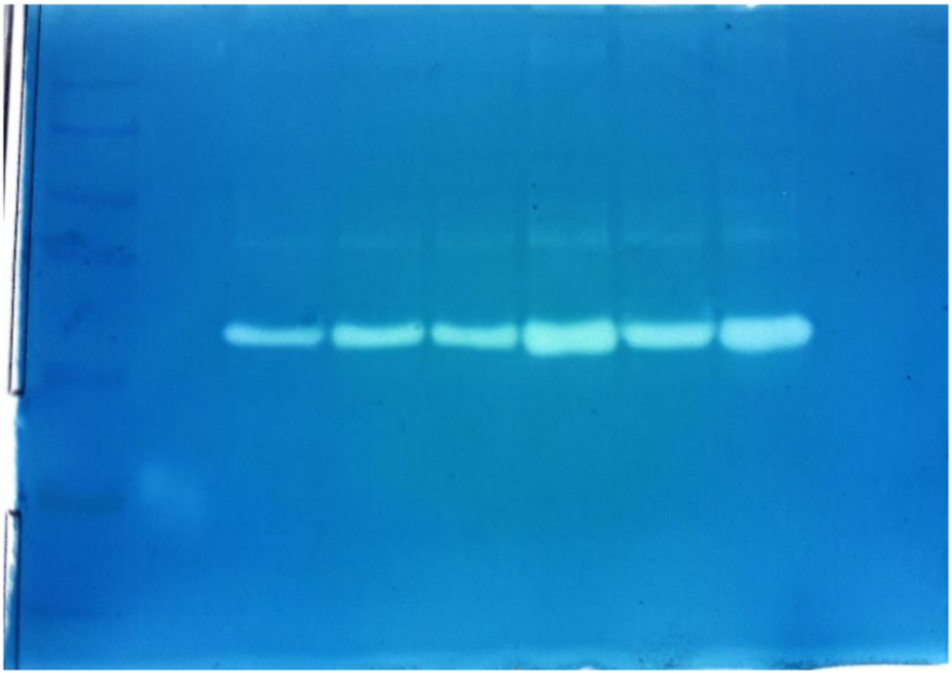

Supplementary Figure S2. Original zymography gel from Figure 3. Lane 1: Molecular weight ladder; Lane 3: Non-diabetic (NDb) M0 CM (conditioned media); Lane 4: NDb M1 CM; Lane 5: NDb M2 CM; Lane 6: Diabetic (Db) M0 CM; Lane 7: Db M1 CM; and Lane 8: Db M2 CM.

98x69mm (300 x 300 DPI)

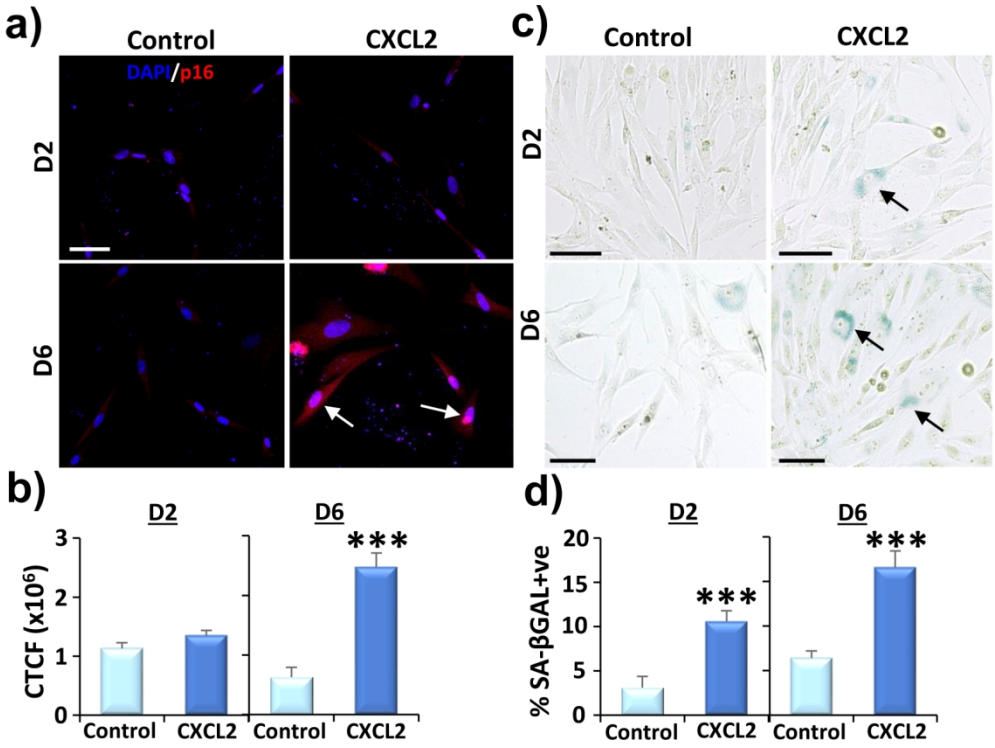

Supplementary Figure S3. Ectopic expression of CXCL2 drives upregulation of senescent markers in human fibroblasts. CXCL2-transfected fibroblasts show increased p16 (red; nuclei, blue) at D6 (day 6) post-transfection (**a-b**). Bar = 50 μm. CTCF = corrected total cell fluorescence. SA-βGAL staining is also increased in CXCL2-transfected fibroblasts at D2 and D6 (**c-d**). Bar = 100 μm. Data show mean +/- SEM. *** = $P < 0.001$.

144x110mm (300 x 300 DPI)

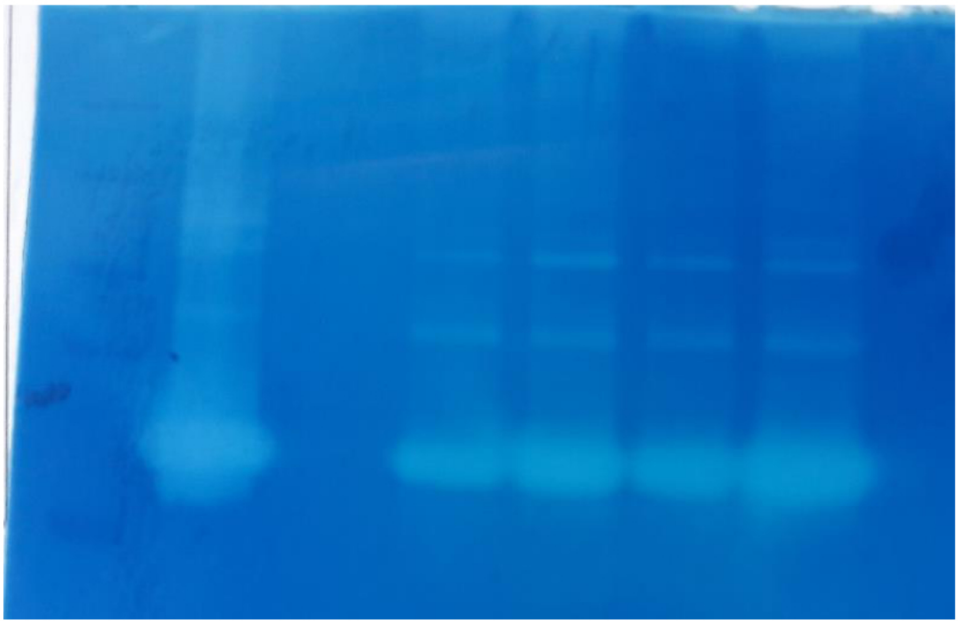

Supplementary Figure S4. Original zymography gel from Figure 4. Lane 1: Molecular weight ladder; Lane 2: MMP2 standard. Lane 4: Control Day 2 CM (conditioned media); Lane 5: Control Day 6 CM; Lane 6: CXCL2 Day 2 CM; Lane 7: CXCL2 Day 6 CM.

95x62mm (300 x 300 DPI)

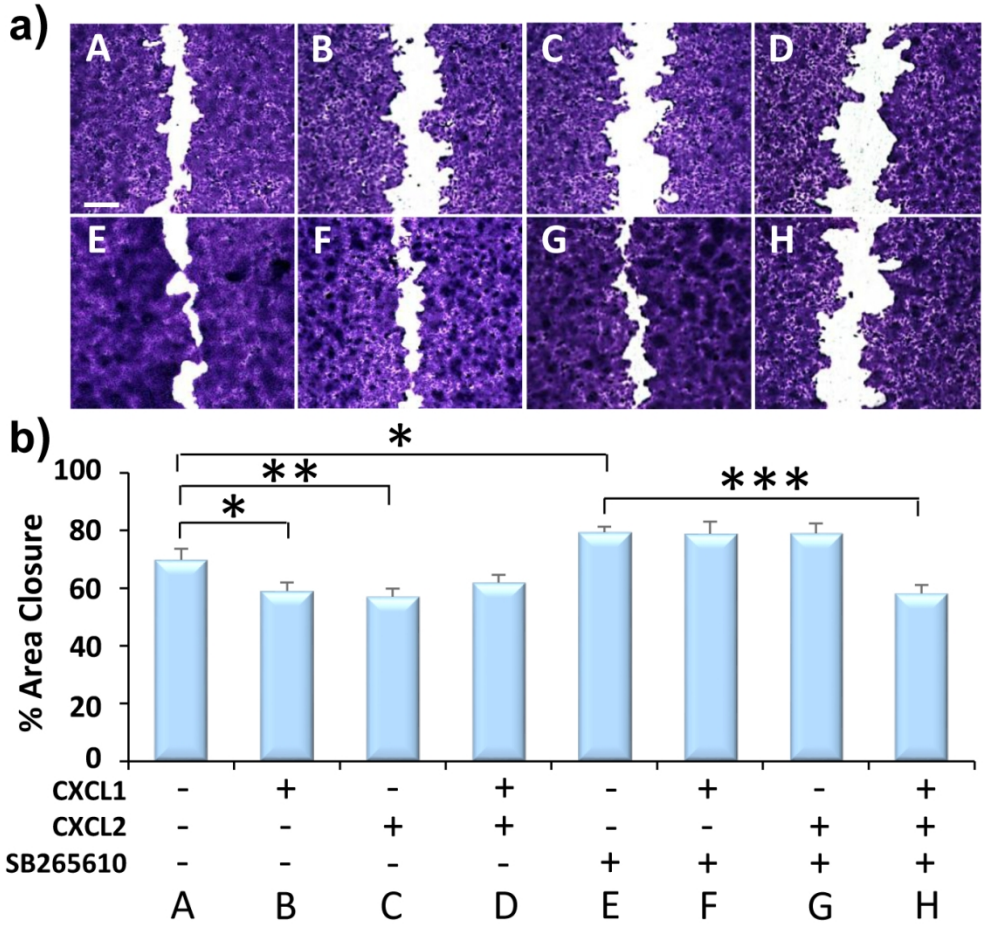

Supplementary Figure S5. CXCR2 inhibition promotes HaCaT scratch migration after 24 hours treatment. The CXCR2 ligands, CXCL1 (A) and CXCL2 (B), impaired *in vitro* HaCaT wound closure (**b**), while treatment with the CXCR2 antagonist, SB265610 (E), accelerated scratch closure (representative of 3 independent experiments). Further, treatment with CXCL1 (F) and CXCL2 (G) with SB265610 independently did not delay scratch closure, whereas SB265610 failed to improve HaCaT migration when both ligands were combined (H). Crystal Violet-stained scratches are presented in **a**. Letters in **a** relate to treatments in **b**. Bar = 250 μm. * = $P < 0.05$, ** = $P < 0.01$, *** = $P < 0.001$.

117x112mm (300 x 300 DPI)

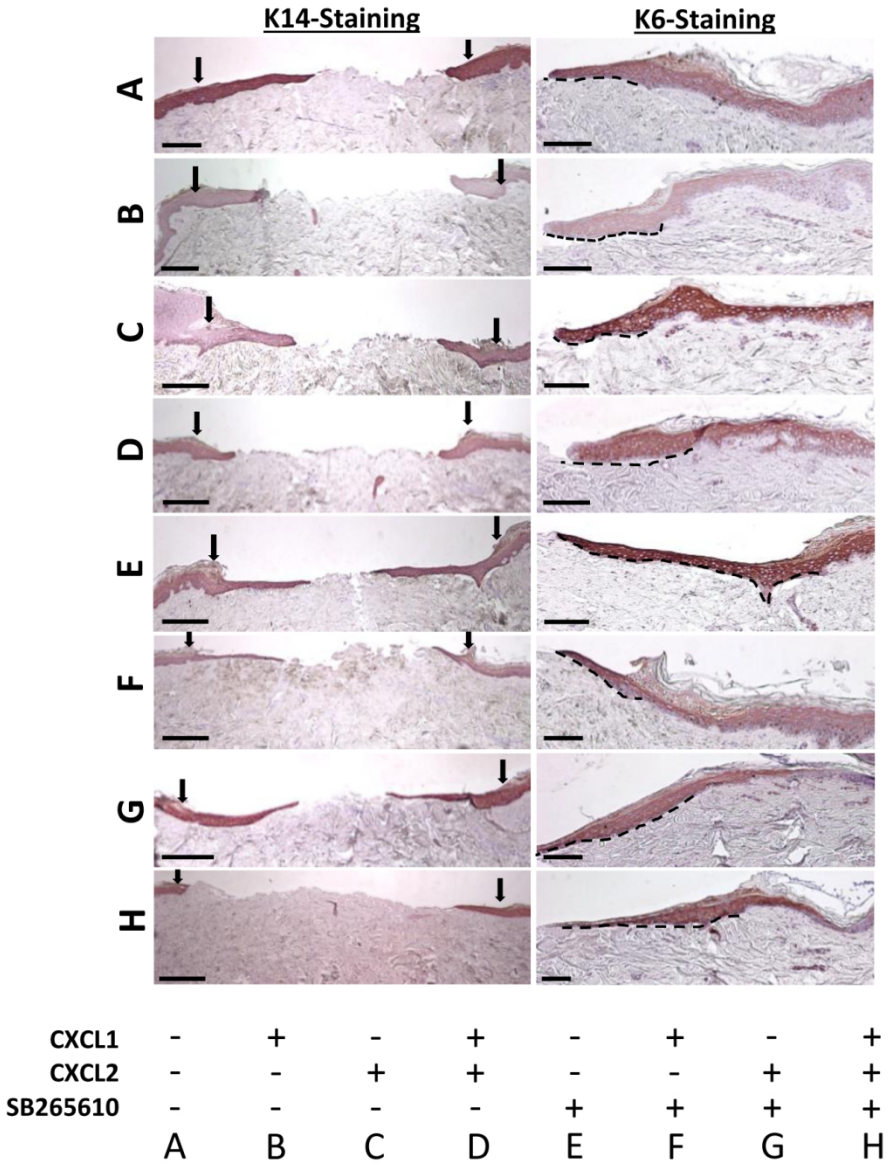

Supplementary Figure S6. Complete representative images for human *ex vivo* wounding experiments. Keratin 14 (K14) and keratin 6 (K6) images of *ex vivo* wounds treated with a vehicle (A), CXCR2 ligands (CXCL1 and CXCL2) or the CXCR2 antagonist, SB265610 (alone, E). Wounds were also treated with combinations of the CXCR2 ligands and SB265610. The panel below the images explains the treatment groups labelled A-H. Arrows depict wound edges (K14). Dotted lines depict neo-epidermis (K6). K14 Bars = 200 μm. K6 Bars = 50 μm. Images representative of 3 human donors.

113x150mm (300 x 300 DPI)